AFFDL-TR-78-10

AD A069286

STRESS INTENSITY DISTRIBUTIONS FOR SURFACE FLAWS UNDER MIXED MODE LOADING

DEPARTMENT OF ENGINEERING SCIENCE AND MECHANICS
VIRGINIA POLYTECHNIC INSTITUTE AND STATE UNIVERSITY
BLACKSBURG, VIRGINIA 24061

MARCH 1978

TECHNICAL REPORT AFFDL-TR-78-10
Final Report March 1976 – December 1977

Approved for public release; distribution unlimited.

20071128055

AIR FORCE FLIGHT DYNAMICS LABORATORY
AIR FORCE WRIGHT AERONAUTICAL LABORATORIES
AIR FORCE SYSTEMS COMMAND
WRIGHT-PATTERSON AIR FORCE BASE, OHIO 45433

NOTICE

When Government drawings, specifications, or other data are used for any purpose other than in connection with a definitely related Government procurement operation, the United States Government thereby incurs no responsibility nor any obligation whatsoever; and the fact that the government may have formulated, furnished, or in any way supplied the said drawings, specifications, or other data, is not to be regarded by implication or otherwise as in any manner licensing the holder or any other person or corporation, or conveying any rights or permission to manufacture, use, or sell any patented invention that may in any way be related thereto.

This report has been reviewed by the Information Office (OI) and is releasable to the National Technical Information Service (NTIS). At NTIS, it will be available to the general public, including foreign nations.

This technical report has been reviewed and is approved for publication.

Gene E. Maddux

GENE E. MADDUX,
Project Engineer

Nelson D. Wolf

NELSON D. WOLF, Acting Chief
Structural Integrity Branch

FOR THE COMMANDER

Ralph L. Kuster, Jr.

RALPH L. KUSTER, JR., Col, USAF
Chief, Structures & Dynamics Division

"If your address has changed, if you wish to be removed from our mailing list, or if the addressee is no longer employed by your organization please notify, AFFDL/FBE, WPAFB, OH 45433 to help us maintain a current mailing list".

Copies of this report should not be returned unless return is required by security considerations, contractural obligations, or notice on a specific document.

AIR FORCE/56780/30 April 1979 — 450

UNCLASSIFIED

SECURITY CLASSIFICATION OF THIS PAGE *(When Data Entered)*

REPORT DOCUMENTATION PAGE		READ INSTRUCTIONS BEFORE COMPLETING FORM
1. REPORT NUMBER AFFDL-TR-78-10	2. GOVT ACCESSION NO.	3. RECIPIENT'S CATALOG NUMBER
4. TITLE *(and Subtitle)* Stress Intensity Distributions for Surface Flaws Under Mixed Mode Loading		5. TYPE OF REPORT & PERIOD COVERED Final Report 6. PERFORMING ORG. REPORT NUMBER
7. AUTHOR(s) C. W. Smith A. Andonian W. H. Peters		8. CONTRACT OR GRANT NUMBER(s) F-33615-76-C-3078 3/1/76 through 12/31/77
9. PERFORMING ORGANIZATION NAME AND ADDRESS Virginia Polytechnic Institute & State University Blacksburg, Virginia 24061		10. PROGRAM ELEMENT, PROJECT, TASK AREA & WORK UNIT NUMBERS Project 2401 Task 01 Work Unit 13
11. CONTROLLING OFFICE NAME AND ADDRESS U.S. Air Force Flight Dynamics Laboratory (FBE) Wright-Patterson Air Force Base Ohio 45433		12. REPORT DATE December 1977 13. NUMBER OF PAGES 46
14. MONITORING AGENCY NAME & ADDRESS*(if different from Controlling Office)* same as No. 11		15. SECURITY CLASS. *(of this report)* Unclassified 15a. DECLASSIFICATION/DOWNGRADING SCHEDULE

16. DISTRIBUTION STATEMENT *(of this Report)*

Approved for Public Release; Distribution Unlimited

17. DISTRIBUTION STATEMENT *(of the abstract entered in Block 20, if different from Report)*

18. SUPPLEMENTARY NOTES

19. KEY WORDS *(Continue on reverse side if necessary and identify by block number)*

Frozen stress
Surface flaws
Stress Intensity Factors
Photoelastic analysis
Part through cracks
Mixed Mode Loads
Part circular flaws

20. ABSTRACT *(Continue on reverse side if necessary and identify by block number)*

Nineteen photoelastic plates, containing part circular flaws inclined at 0°, 30° and 60° to the plate surface and covering an aspect ratio range of 0.10 to 0.29 and a relative depth range of 0.20 to 0.70 were loaded parallel to the plate surfaces and analysed by the "frozen stress" method. Photoelastic data were fed into a digital computer programmed to provide estimates of , K_2 and K_3, the stress intensity factors for loading modes I, II and III. Results revealed that:

i) For the part circular flaw shape, normalized K_1 values reveal a maximum

DD FORM 1 JAN 73 1473 EDITION OF 1 NOV 65 IS OBSOLETE

UNCLASSIFIED

SECURITY CLASSIFICATION OF THIS PAGE *(When Data Entered)*

20. value away from the point of maximum flaw penetration which shifts further away with increasing relative flaw depth.

ii) Strong effects of inclination angle and relative depth were observed but the influence of aspect ratio in the range studied here was small.

iii) K_3 effects were negligible.

Results were qualitatively compared with analytical results for similar problems.

FOREWORD

This report was prepared by the Photoelasticity and Fracture Laboratory, Department of Engineering Science and Mechanics, Virginia Polytechnic Institute and State University, Blacksburg, Virginia for the Structural Integrity Branch, Structures & Dynamics Division, Air Force Flight Dynamics Laboratory, Wright-Patterson AFB, OH 45433, under contract F33615-76-C-3078, Project 2401, "Structural Mechanics", work unit 24010113. The contract was administered by G.E. Maddux, Project Engineer, AFFDL/FBE.

The research was conducted between 1 March, 1976, and 31 December, 1977. This final report was submitted by the authors C.W. Smith, A. Andonian and W.H. Peters in December of 1977 for AFFDL review.

The authors wish to acknowledge the advice and counsel of G.E. Maddux during the project.

TABLE OF CONTENTS

LIST OF FIGURE TITLES

SECTION I

INTRODUCTION

The most frequently encountered crack geometry in the aerospace field is the surface flaw in bodies of finite thickness. These flaws may be initiated in a variety of ways from surface imperfections, and their growth under cyclic loading is believed to result in more failures of aerospace structural components than from any other cause. Although an analytical treatment for the local field around a surface flaw in a half space was provided by Irwin in 1962 (1) the problem of the surface flaw in a body of finite thickness has resisted efforts of applied mathematicians to render it tractable in the full field closed form sense, even for the elastic case. In recent years, capitalizing on the speed and storage capacity of modern digital computers, various numerical techniques (2),(3) have been focused on the problem and progress in this direction is continuing (4). However, rigorous convergence proofs for three dimensional cracked body problems are difficult to achieve, and research programs are now uniformly requiring computer code verification on an experimental basis in order to validate numerical analyses.

Several years ago, the senior author and his associates began to develop (5-7) an experimental technique based upon an idea of G. R. Irwin for direct measurement of stress intensity factors (SIFs) photoelastically. They adapted the idea to the so called "frozen stress" method, which they then combined with an elementary least squares digital computer program for estimating SIF distributions for three dimensional cracked body problems. The early form of the technique was identified by the Society for Experimental Stress Analysis as a viable approach to three dimensional cracked body problems and was featured in the lead chapter of a recent SESA monograph (8) on Experimental Fracture Mechanics. The method has been modified and refined since that time (9-15) and has been successfully applied to several surface flaw problems to date (7), (16-30).

A problem which has received only limited attention (31) in the literature deals with the surface flaw in a finite body under mixed mode loading. Absence of information on this subject is not unexpected since this problem is substantially more complex than the pure Mode I problem discussed above. The study described in the sequel is concerned with the application of the frozen stress technique noted above to the Mixed Mode Surface Flaw problem in which part-circular flaw geometries were employed.

SECTION II

ANALYTICAL CONSIDERATIONS

The main quantity obtained from photoelastic analysis is the maximum shearing stress in a plane normal to the direction of travel of the polarized light field. In this section we develop the analytical background for converting this information into SIF values.

It has been shown (32) that the stresses near the border of an elliptical crack, when expressed in coordinates in a plane perpendicular to the border, have the same form as the stresses in a plane perpendicular to the border of a crack with a straight front. For a crack with a circular front, the same type of results had been obtained by Sneddon (33). This form of the stresses is further verified by the work of Thresher and Smith (34) for the part circular crack.

Consider an infinite plate with finite thickness which is subjected to uniaxial loading. The stress distribution near a part-circular crack, which is inclined to the plate boundary at an angle β, can be found using the following arguments.

The geometry is shown in Figure 1. Based on previous experimental work the infinite plate assumption appears valid for $2m < 0.30\ w$ and $L > 3w$ where $2m$ is the crack length, w is the plate width, and L is the plate length.

The orthogonal coordinate system nzt used in this problem (see Figure 2) is a local frame and it will move along the leading edge of the part circular crack, such that z will always be perpendicular to the crack surface, and n and t will define the crack surface and will remain perpendicular and tangent respectively to the flaw border.

It is clear that the three modes of loading Mode I, Mode II, and Mode III are present at any point along the crack front.

The stress distribution near the part-circular crack, corresponding to the opening mode of deformation can be taken as (15).

$$\sigma_{nn} = \frac{K_1}{(2\pi r)^{1/2}} \cos\frac{\theta}{2}\left[1 - \sin\frac{\theta}{2}\sin\frac{3\theta}{2}\right] - \sigma^1_{nn}$$

$$\sigma_{zz} = \frac{K_1}{(2\pi r)^{1/2}} \cos\frac{\theta}{2}\left[1 + \sin\frac{\theta}{2}\sin\frac{3\theta}{2}\right] - \sigma^1_{zz}$$

$$\tau_{nz} = \frac{K_1}{(2\pi r)^{1/2}} \sin\frac{\theta}{2}\left[\cos\frac{\theta}{2}\cos\frac{3\theta}{2}\right] - \sigma^1_{nz} \qquad (1)$$

where K_1 is the Mode I SIF and the coordinates r and θ are shown in Figure 2. σ^1_{ij} represent the contribution of the Mode I regular stress

field to the measurement zone which is taken far enough from the crack tip to avoid a non-linear zone very near the tip. While they may generally be regarded as expressible in Taylor Series Expansions, it turns out that only the leading terms of said series are necessary so that σ_{ij}^1 are constants for a given point in the flaw border but vary from point to point. Stresses corresponding to the Mode II can be taken as

$$\sigma_{nn} = -\frac{K_2}{(2\pi r)^{1/2}} \sin\frac{\theta}{2}\left[2 + \cos\frac{\theta}{2}\cos\frac{3\theta}{2}\right] - \sigma_{nn}^2$$

$$\sigma_{zz} = \frac{K_2}{(2\pi r)^{1/2}} \sin\frac{\theta}{2}\cos\frac{\theta}{2}\cos\frac{3\theta}{2} - \sigma_{zz}^2$$

$$\tau_{nz} = \frac{K_2}{(2\pi r)^{1/2}} \cos\frac{\theta}{2}\left[1 - \sin\frac{\theta}{2}\sin\frac{3\theta}{2}\right] - \tau_{nz}^2 \qquad (2)$$

where K_2 and σ_{ij}^2 are analogous to K_1 and σ_{ij}^1.

And finally the stresses corresponding to the Mode III loading can be taken as

$$\tau_{nt} = -\frac{K_3}{(2\pi r)^{1/2}} \sin\frac{\theta}{2} - \tau_{nt}^3$$

$$\tau_{zt} = \frac{K_3}{(2\pi r)^{1/2}} \cos\frac{\theta}{2} - \tau_{zt}^3 \qquad (3)$$

with K_3 and σ_{ij}^3 analogous to K_1 and σ_{ij}^1.

If the above modes of loading are superimposed, one gets the following stress distribution in a plane perpendicular to the crack front (the n-z plane)

$$\sigma_{nn} = \frac{K_1}{(2\pi r)^{1/2}} \cos\frac{\theta}{2}\left[1 - \sin\frac{\theta}{2}\sin\frac{3\theta}{2}\right]$$

$$- \frac{K_2}{(2\pi r)^{1/2}} \sin\frac{\theta}{2}\left[2 + \cos\frac{\theta}{2}\cos\frac{3\theta}{2}\right] - \sigma_{nn}^o$$

$$\sigma_{zz} = \frac{K_1}{(2\pi r)^{1/2}} \cos\frac{\theta}{2}\left[1 + \sin\frac{\theta}{2}\sin\frac{3\theta}{2}\right] \qquad (4)$$

$$+ \frac{K_2}{(2\pi r)^{1/2}} \sin\frac{\theta}{2}\cos\frac{\theta}{2}\cos\frac{3\theta}{2} - \sigma_{zz}^o$$

$$\tau_{nz} = \frac{K_1}{(2\pi r)^{1/2}} \sin\frac{\theta}{2}\cos\frac{\theta}{2}\cos\frac{3\theta}{2}$$

$$+ \frac{K_2}{(2\pi r)^{1/2}} \cos\frac{\theta}{2}\left[1 - \sin\frac{\theta}{2}\sin\frac{3\theta}{2}\right] - \tau^{o}_{nz}$$

which are independent of Equations (3).

While σ^{o}_{ij} has no influence upon the singular stress field itself, it does alter the isochromatic fringe pattern, which is proportional to the maximum in-plane shearing stress.

From the stress field given in Equations 4, the maximum shearing stress in the plane perpendicular to the crack front, nz, can be obtained using

$$(\tau_{nz})_{max} = \left[\left(\frac{\sigma_{zz}-\sigma_{nn}}{2}\right)^2 + \tau^2_{nz}\right]^{1/2} \qquad (5)$$

and, truncating to the same order as Equation 4, one gets

$$(\tau_{nz})_{max} = \frac{A}{r^{1/2}} + B \qquad (6)$$

where

$$A = \left\{\frac{1}{8\pi}\left[(K_1 \sin\theta + 2K_2\cos\theta)^2 + (K_2\sin\theta)^2\right]\right\}^{1/2}$$

and

$$B = B\,(\theta, K_1, K_2, \sigma^{o}_{ij})$$

Photoelastically, the maximum shearing stress (in the nz plane) is determined from the stress optic law

$$\tau_{max} = \frac{fn'}{2t'} \qquad (7)$$

where

f is the photoelastic fringe constant for the material
t' is the thickness of the slice measured parallel to the direction of the light, and
n' is the isochromatic fringe order.

Now, in general, the effect of σ^{o}_{ij} involves both a folding and a change in eccentricity of the fringe loops (13). If folding occurs, θ_m, the angle along which the distance to a fringe from the crack tip is greatest, will vary with the fringe order n' and one must plot θ_m vs r/a and extrapolate to the origin in order to obtain θ^{o}_{m}, the value of θ_m associated with K_1 and K_2. In the present problem θ_m was constant over the data range in the fashion indicated qualitatively by Figure 3.

Upon computing

$$\lim_{\substack{r\to 0 \\ \theta\to\theta_m^o}} \{(8\pi r)^{1/2} \frac{\partial(\tau_{nz})_{max}}{\partial\theta} (K_1 \quad K_2, r, \theta, \sigma_{ij}^o)\} = 0 \tag{8}$$

one obtains

$$(\frac{K_2}{K_1})^2 - \frac{4}{3}(\frac{K_2}{K_1}) \cot 2\theta_m^o - \frac{1}{3} = 0 \tag{9}$$

Since θ_m^o can be measured experimentally (K_2/K_1) can be calculated from Equation 9. Then by combining the stress-optic law with a modified form of Equation 6.

$$(\tau_{nz})_{max} = \frac{fn'}{2t'} = \frac{K_{AP}^*}{(8\pi r)^{1/2}} \tag{10}$$

where $K_{AP}^* = (\tau_{nz})_{max}(8\pi r)^{1/2}$ is defined as the "apparent" SIF.

$$\text{Thus } K_{AP}^* = [(K_{1AP} \sin\theta_m + 2K_{2AP} \cos\theta_m)^2 + (K_{2AP} \sin\theta_m)^2]^{1/2} \tag{11}$$

and one can solve for the individual values of K_1 and K_2.

In order to do this, one must obtain

$$K^* = [(K_1 \sin\theta_m^o + 2K_2 \cos\theta_m^o)^2 + (K_2 \sin\theta_m^o)^2]^{1/2}$$

from K_{AP}^* by plotting $K_{AP}^* = (\tau_{nz})_{max}(8\pi r)^{1/2}$ vs $(\frac{r}{a})^{1/2}$ identifying a linear zone, and extrapolating to the origin, which will yield K^*. A typical set of fringe data and SIF determination is given in Figure 4. Once K^*, K_2/K_1, and θ_m^o are known K_1 and K_2 can be calculated which then can be normalized using proper quantities.

Note that the above approach utilizes a two parameter (A, B) model, since the linear zone of Equation 10 can be located experimentally. However, if one cannot locate such a zone experimentally then additional terms leading to an equation of the form

$$\tau_{max} = \frac{A}{r^{1/2}} + \sum_{n=o}^{\infty} B_n r^{n/2} \tag{12}$$

with suitable truncation criteria must be considered. Since such criteria are not yet established, this latter approach is avoided where possible and was not necessary in the studies described in the sequel.

The stress distribution in a plane perpendicular to the crack surface and tangent to the crack front (zt plane) or in a plane parallel to the zt plane can be found from Equations 4.

$$\sigma_{zz} = \frac{K_1}{(2\pi r)^{1/2}} \cos\frac{\theta}{2}\left[1 + \sin\frac{\theta}{2}\sin\frac{3\theta}{2}\right]$$

$$+ \frac{K_2}{(2\pi r)^{1/2}} \sin\frac{\theta}{2}\left[\cos\frac{\theta}{2}\cos\frac{3\theta}{2}\right] - \sigma^{o}_{zz} \qquad (13)$$

In order to arrive at a value for σ_{zz}, prior experiments by the authors indicate that the usual assumption of plane strain (for the plane problem) may not be valid here. However, if one assumes a state of nearly generalized plane strain such that the value of ε_{tt} can be considered constant over a portion of the length of the flaw border, then the observed state of varying transverse constraint along the flaw border can be approximated rather well. Thus, we assume

$$\varepsilon_{tt} = \frac{\sigma_{tt} - \nu(\sigma_{nn} + \sigma_{zz})}{E} \simeq \bar{\varepsilon} \qquad \text{whence}$$

$\sigma_{tt} \simeq E\bar{\varepsilon} + \nu(\sigma_{nn} + \sigma_{zz})$ where $\bar{\varepsilon}$ may be adjusted at intervals along the flaw border and where

$$\sigma_{nn} = \frac{K_1}{(2\pi r)^{1/2}} \cos\frac{\theta}{2}\left[1 - \sin\frac{\theta}{2}\sin\frac{3\theta}{2}\right]$$

$$- \frac{K_2}{(2\pi r)^{1/2}} \sin\frac{\theta}{2}\left[2 + \cos\frac{\theta}{2}\cos\frac{3\theta}{2}\right] - \sigma^{o}_{nn}$$

For $\nu = \frac{1}{2}$ (as in the present experiments)

$$\sigma_{tt} = \frac{K_1}{2(2\pi r)^{1/2}}\left\{\cos\frac{\theta}{2}\left[1 + \sin\frac{\theta}{2}\sin\frac{3\theta}{2}\right] + \cos\frac{\theta}{2}\left[1 - \sin\frac{\theta}{2}\sin\frac{3\theta}{2}\right]\right\}$$

$$- \frac{K_2}{(2\pi r)^{1/2}} \sin\frac{\theta}{2} - \sigma^{o}_{tt} + E\bar{\varepsilon} \qquad (13a)$$

Moreover, from Mode III, we have,

$$\tau_{zt} = \frac{K_3}{(2\pi r)^{1/2}} \cos\frac{\theta}{2} - \tau^{o}_{zt} \qquad (13b)$$

$$(\tau_{zt})_{max} = \left[\left(\frac{\sigma_{zz} - \sigma_{tt}}{2}\right)^2 + \tau^2_{zt}\right]^{1/2}$$

Consider the line normal to the crack surface which passes through the crack tip in the zt plane. For this case $\theta = \frac{\pi}{2}$, and when substituted in Equations 13, 13a and 13b, there results

$$\sigma_{zz} = \frac{1}{4(\pi r)^{1/2}}\left[3K_1 - K_2\right] - \sigma^{o}_{zz}$$

$$\sigma_{tt} = \frac{1}{2(\pi r)^{1/2}} [K_1 - K_2] - \sigma^o_{tt} + E\bar{\varepsilon} \tag{14}$$

$$\tau_{zt} = \frac{K_3}{2(\pi r)^{1/2}} - \tau^o_{zt}$$

then

$$(\tau_{zt})_{max} = \frac{C}{r^{1/2}} + D \tag{15}$$

where

$$C = \frac{1}{(4\pi)^{1/2}} [\frac{1}{16} (K_1 + K_2)^2 + K_3^2]^{1/2}$$

and

$$D = D\ (K_1,\ K_2,\ K_3,\ E\bar{\varepsilon} \text{ and } \sigma^o_{ij})$$

Now by combining the stress optic law with a modified form of Equation 15

$$(\tau_{zt})_{max} = \frac{fn'}{2t'} = \frac{K^{**}_{AP}}{(8\pi r)^{1/2}}$$

where

$$K^{**}_{AP} = \sqrt{2}\ [\frac{1}{16} (K_{1AP} + K_{2AP})^2 + K^2_{3AP}]^{1/2}$$

the value of K_3 can be obtained.

In order to do this, one must obtain

$K^{**} = \sqrt{2}\ \{\frac{1}{16} (K_1 + K_2)^2 + K_3^2\}^{1/2}$ from K^{**}_{AP} by plotting a

$K^{**}_{AP} = (\tau_{zt})_{max}(8\pi r)^{1/2}$ vs $(r/a)^{1/2}$,

identifying a linear zone, and extrapolating to the origin, which will yield K**.

SECTION III

THE EXPERIMENTS

"Frozen stress" experiments require that the model material exhibit certain special characteristics in addition to the optical transparency required of all photoelastic materials. Stress freezing materials behave in a Kelvin-like manner (Figure 5) at room temperature. However, when heated to a certain temperature, known as the "critical" temperature, the anelastic coefficient $\mu \to 0$, and the material becomes linearly elastic, exhibiting an elastic modulus over two orders of magnitude below the room temperature value and an isochromatic sensitivity twenty-five times greater than at room temperature. If the cracked body is heated to critical temperature, loaded and cooled slowly under load, the recovery effects upon unloading are negligible due to the difference in modulus and isochromatic sensitivity between critical and room temperature. In fact the model may be sliced (and this is done parallel to the nz plane [Figure 1]) without altering the isochromatic or deformation patterns imposed above critical temperature. Thus "frozen stress" is a misnomer in the sense that live or macrostresses are not trapped in the body, but rather deformation fields and the isochromatic evidence of live stress above critical temperature.

A series of 19 photoelastic models were prepared in accordance with Table I. Cracks were simulated with thin sawn slits tapered with a 30° vee tip to a root radius of 2.5×10^{-4}mm. Such geometries had been shown analytically (35) and experimentally (10) to yield SIF estimates to within 2% of natural cracks. Mixed mode fields were then frozen into 17 of these models and primary slices were removed near the crack tip along the flaw border parallel to the nz plane. Isochromatics were read from these slices by placing them in a circularly polarized white light field in a bath of matching index fluid, and reading tint of passage using the Tardy Method along predetermined directions. Typical fringe patterns are shown in Figure 6. Optical data were then fed into a least squares digital computer program for establishing the curve of best fit, from which K* estimates were obtained by extrapolation as in Figure 4. These values were then converted to K_1 and K_2 values analytically. Secondary slices were then obtained from the primary slices and analyzed in a similar manner for K_3.

SECTION IV

RESULTS

Test geometries and loads for all sixteen experiments are given in Table I according to increasing a/T'. Test 4 represents an average of four identical tests and so nineteen tests were conducted altogether. SIF distributions for Modes I and II are presented in Figures 7 through 22. The normalizing factor $\bar{K}_1 = \bar{\sigma}(\pi a)^{1/2}\sin^2\beta$, is the Mode I SIF for a through straight front crack in an infinite body whose plane is inclined at an angle β to the remote uniform stress $\bar{\sigma}$. Similarly, $\bar{K}_2 = \bar{\sigma}(\pi a)^{1/2}$ sin β cos β is the Mode II SIF for the same problem. Consequently, the normalizing factors do not vary along the flaw border.

There are several points which the authors wish to make regarding the results of Figures 7 through 22. First, it has been pointed out by other investigators (36), (37) that the calculations used in this type of approach are quite sensitive to values of θ_m, especially for $\theta_m \simeq 90°$ (Fig. 3). In order to assess this effect upon the present results, four "identical" tests were conducted (Tests 4) for the geometry expected to produce the highest scatter due to the sensitivity to θ_m. Results are given in Figure 7 showing the average values with a scatter band for the data from the four tests. These results indicate that, indeed, when the method is applied to mixed mode studies where θ_m is measured rather than assumed (as for Mode I) the resulting accuracy in measuring both Modes I and II is reduced from the usual scatter of $\pm$ 5% for the pure Mode I case to as large as $\pm$ 12% for Mixed Mode problems with artificial cracks at the point of maximum flaw penetration.

Due to limitations on cutter sizes for producing the part circular flaws, it was not possible to hold two of the variables β, a/T', a/2m constant while varying the other one. In order to cover a range of interest, three levels of a/T' were treated, two values of β and two levels of a/2m. With this approach, it turned out that when β was increased from 30° to 60°, an increase in a/T' also occurred. Although the influence of the inclination of the remote stress to the crack surface was normalized out using $\bar{K}$ values, the influence of the inclination of the plate surfaces to the Mixed Mode Components remains embedded in the data. In four of the tests (13 thru 16) Figs. 20-22, a study of the influence of 2m/w was conducted.

Within the above limitations, the following trends can be observed:

Effect of a/T', β - Tests 2, 4, 6, 7 and 11 (Figures 9, 7, 12, 13, 18 respectively) show a continuously increasing a/T' with little change in a/2m. Some of these tests (2 and 6) were for $\beta = 30°$ and the others (4, 7 and 11) were for $\beta = 60°$. Viewing these tests collectively, the only consistent result appears to be that maximum values of $K_1/\bar{K}_1$ and $K_2/\bar{K}_2$ do not occur at maximum flaw penetration for any case. No significant trends, however, are noted. On the other hand, if one separates the tests according to values of β, (i.e. 2 and 6 and 4, 7, 11) definite trends do appear. In both sets, the magnitude of $K_1/\bar{K}_1$ increases with a'/T and shifts away from the point of maximum flaw penetration. Also, while $K_1/\bar{K}_1 > K_2/\bar{K}_2$ for $\beta = 30°$, the reverse is true for $\beta = 60°$. The location of the maximum value of $K_2/\bar{K}_2$ does not shift, however, as it did for $K_1/\bar{K}_1$. This could be due to the interaction between the influence

of the angle α (Fig. 1) (which appears in the second order cartesian tensor transformation of the remote stress into its pointwise Mode II component along the flaw border) with the free boundary effects. (Said angle α is not present in the Mode I transformation).

Effect of a/2m - Tests 1 and 2 (Figs. 8, 9), 3 and 4 (Figs. 10, 7), and 9 and 10 (Figs. 15, 16) represent shallow, moderately deep and deep flaws of about the same a/T' in pairs, but involving significant changes in a/2m. These tests do not reveal any identifiable trends insofar as increasing or decreasing of the normalized SIF values with increasing a/2m. The most significant result appears to be that $K_1/\bar{K}_1$ does not have a maximum value at the point of maximum flaw penetration in any of these tests but rather at α/α_{max} of 1/3 to 1/2. The absence of trends in the normalized SIF magnitudes again suggests a strong role of the orientation of the external plate surfaces which is not accounted for in the current normalizing procedure.

Effect of Plate Width - Four tests (13-16, Figs. 20-22) were conducted in order to assess the gross influence of plate width. As seen in Figure 22, Tests 15 and 16 indicate the increase in 2m/w from 0.31 to 0.36 results in a reduction in $K_1/\bar{\sigma}(\pi a)^{1/2}$ of about 10% at the point of maximum flaw penetration. However, if one compares the average of the results of tests 9 and 10 (Fig. 17) with the result of test 14 (Fig. 21), one finds the width influence of 2m/w = 0.44 to still be small. Moreover, comparisons between tests 9 and 13 (Figs. 15, 20) (which have a/T' and a/2m values in the same range suggests that the width effect, while significant at 2m/w = 0.64 for $K_1/\bar{K}_1$, is negligible for $K_2/\bar{K}_2$.

Photoelastic analysis of secondary slices for K_3 determination revealed that, for the range of geometrics studied in the present program, the magnitude of K_3 was so small that it was swamped by experimental scatter and thus no K_3 values are reported herein.

SECTION V

DISCUSSION

The authors are aware of only two analytical investigations which appear to bear in any way upon the studies conducted here. One such study (34) conducted by F. W. Smith and Thresher, focused upon the part circular flaw shape under Mode I loading and was generally verified by the authors experimentally in an earlier study (23) for moderate to deep flaws. The exact location of maximum Mode I values was not clear from the verification tests, however, due to slight loading dysymmetry in the experiments. Tests 15 and 16, however, (Fig. 22) clarify this point. Using quadratic interpolation of the results of (34) they are compared with the Mode I results of this study in Figures 23 and 24. Differences in these comparisons would be attributed to the difference in orientation of the plate surfaces to the Mode I direction (i.e. normal to crack surface). As expected these differences are larger for $\beta = 30°$, Fig. 23, than for $\beta = 60°$, Fig. 24. A second difference is that the analytical study does not predict maximum SIF values at locations other than at maximum flaw penetration. On the other hand, a second analytical study by F. W. Smith and Sorensen (31), noted earlier, was carried out on semi-elliptical shaped surface flaws using uniformly distributed stress distributions normal to the flaw surface and parallel to the surface dimension of the flaw. Here, as in (34) the plate surface was normal to the crack surface. These studies did show a shift in the location of the maximum normalized SIF away from the point of maximum flaw penetration for low aspect ratio shallow to moderately deep flaws but not for deep flaws.

In separate investigations (26-30) the authors have found that, in general, stable, or fatigue flaw growth in three dimensional problems is generally not self-similar, nor do real flaw shapes assume the form of simple curves. Moreover, Sommer et al (38) have shown that surface flaws in metals, if initiated by part circular slots, tend to grow into nearly semi-circular shapes, then semi-ellipses and finally a bulge appears near the region of $(K_1/\bar{K}_1)$ maximum in the present study which distorts the shape from a semi-ellipse. Collectively the above results suggest that natural flaw shapes in three dimensional cracked body problems are strongly influenced by a variation in crack growth resistance along the flaw border, which the authors conjecture to be primarily due to a variation in triaxial constraint along the flaw border. Moreover, the authors have found (26-30) that, in complex three dimensional problems, the flaws will assume shapes which tend to minimize the SIF gradient along such borders. However, due to constraint variations along the flaw borders, the SIF will not be uniform even for naturally grown flaws.

The present study focused upon part circular slots exclusively, and while such shapes are commonly employed as fatigue crack starters, they cannot represent the myriad of flaw shapes seen in real fatigue cracks. Nevertheless, the shift of the point of maximum SIF away from the point of maximum flaw penetration in the part circular cracks can be partially explained by noting that the natural flaw shape is relatively deeper than part circular cracks in the region where the SIF's peak in the part circular flaw results. If such part circular cracks were permitted to grow naturally, they will tend to grow more in such regions reducing the local SIF there.

It should be emphasized that the above discussion is confined to stable flaw growth as experienced in fatigue.

SECTION VI

SUMMARY and CONCLUSIONS

After developing appropriate analytical expressions for mixed mode loadings in three dimensional cracked body problems, a series of "frozen stress" photoelastic experiments were conducted on plates containing narrow, part-circular slots inclined at an angle β to the plate surface and loaded in uniform simple tension parallel to the lateral plate boundaries. Frozen stress data were extracted from slices taken mutually orthogonal to the flaw surfaces and flaw borders, and inserted into a digital computer program for estimating SIF distributions along the flaw borders. These results were evaluated and compared with a modified form of an existing Mode I analysis. The following conclusions are drawn:

1) Effect of β (Fig. 1): Although the influence of β, or, more precisely, the angle between the direction of the remote stress and the crack plane as sensed through an ordinary second order cartesian tensor transformation at the crack tip of the remote stress was normalized out, the effect of the orientation of the plate surfaces relative to the crack plane remained in the data and significantly altered the SIF distributions for the two values of β studied. The main effect on the $K_I/\bar{K}_I$ and $K_2/\bar{K}_2$ magnitudes was to reverse their order in going from $\beta = 30°$ to $\beta = 60°$.

2) Effect of a/T': As a/T' was increased from 0.2 to 0.7, the values of $K_1/\bar{K}_1$ were found to increase also. Moreover, the SIF distribution also changed, shifting the point of maximum $K_1/\bar{K}_1$ further from the point of maximum flaw penetration with increasing depth. Such shifts were not observed in $K_2/\bar{K}_2$.

3) Effect of a/2m: Test results were confined to $0.10 < a/2m < 0.30$. In this range, doubling the value of a/2m did not produce any significant data trends.

4) Effect of plate width: Tests were conducted here and elsewhere (23) which established that for values of $2m/w \leq 0.30$, influence on the SIF distributions of the side boundaries of the plate were within experimental scatter.

5) SIF Distributions: The shift in the point of maximum $K_1/\bar{K}_1$ away from the point of maximum flaw penetration is a real and consistently observed effect.

6) Role of K_3: For the geometrical ranges studied here, the role of K_3 was insignificant.

In applying the results of this study, it is important to note that this study showed that, in applying the frozen stress method in mixed mode analysis, where θ_m^o was measured, (rather than assumed) scatter in the data approximately doubled (i.e. $\pm$ 12% rather than $\pm$ 5%). Moreover, while these results are believed to be correct trends and distributions to within the above accuracy, it must be kept in mind that the part circular flaw shape is not necessarily the preferred shape of a naturally growing fatigue crack, and consequently, may lead to higher SIF gradients along the flaw borders than for other flaw shapes. Nevertheless, these results are believed to be the most practical and comprehensive for the problem studied that are currently available. The authors, however, do not recommend extrapolation to significantly different flaw geometries.

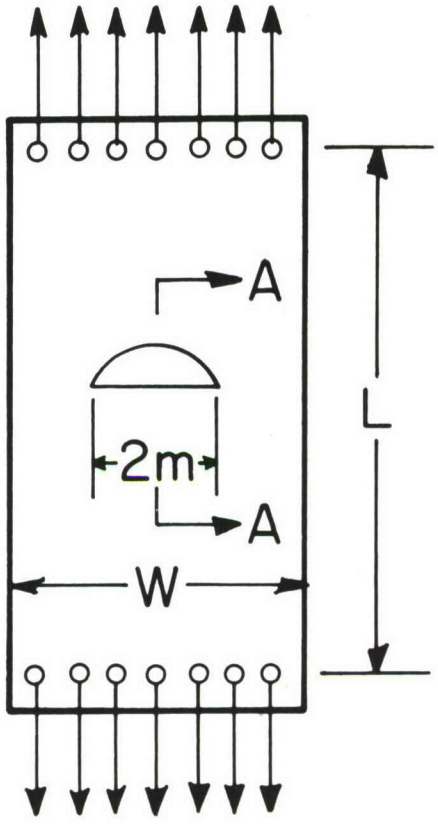

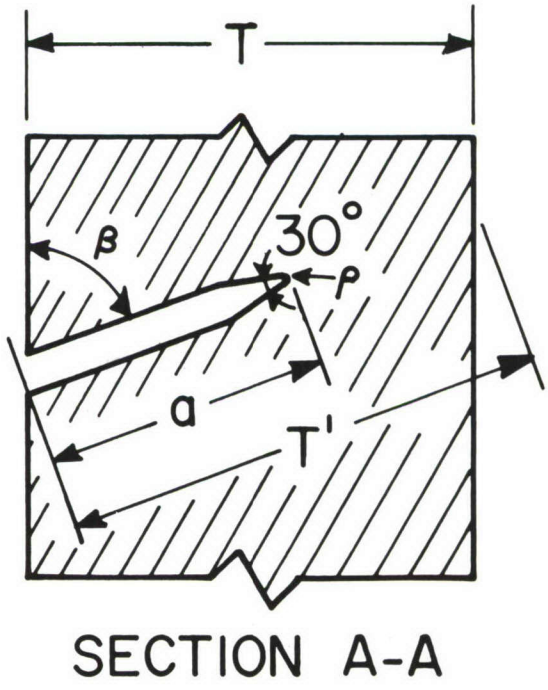

Figure 1) Problem Geometry

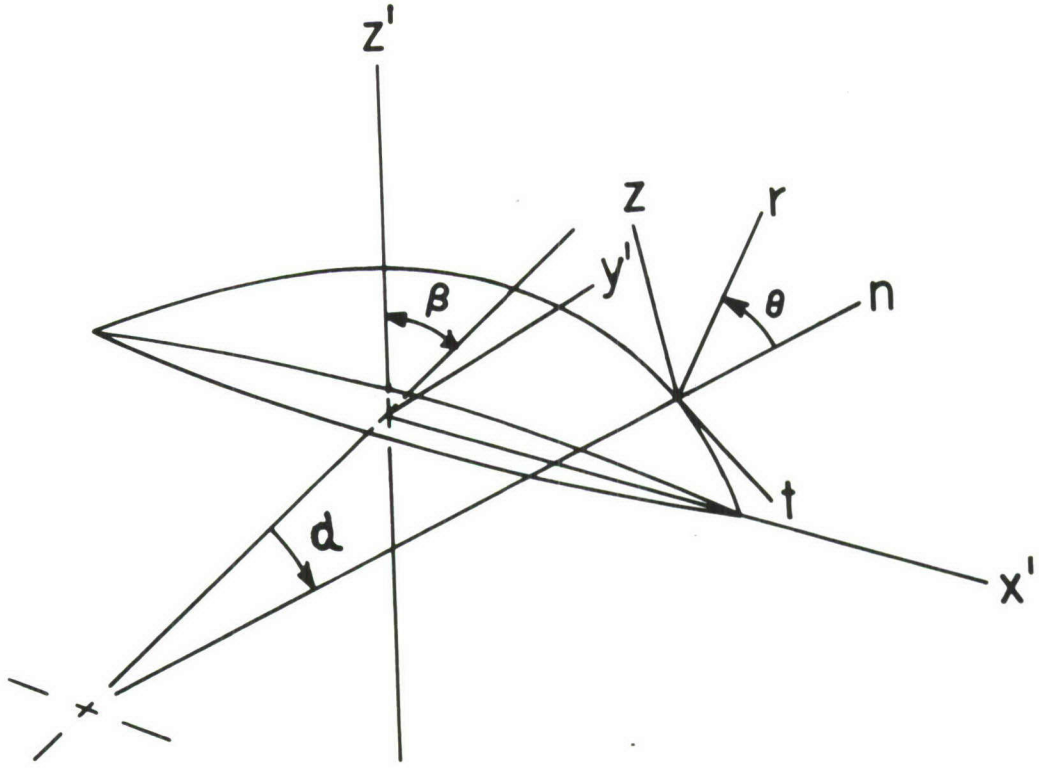

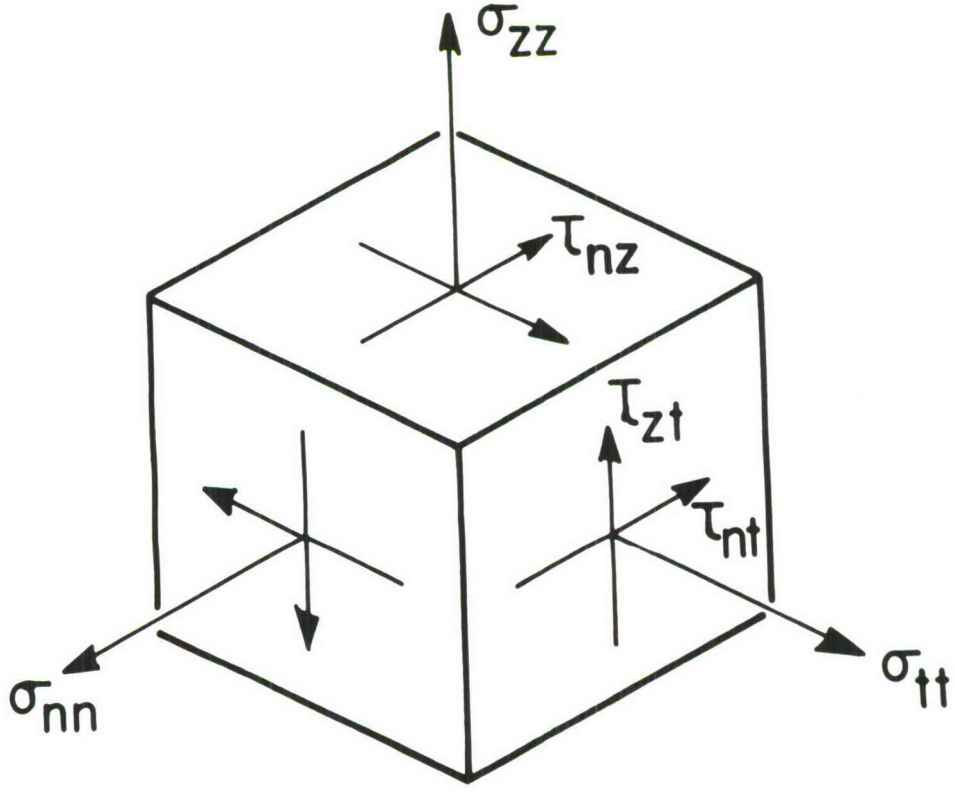

Figure 2) Coordinate and Stress Notation

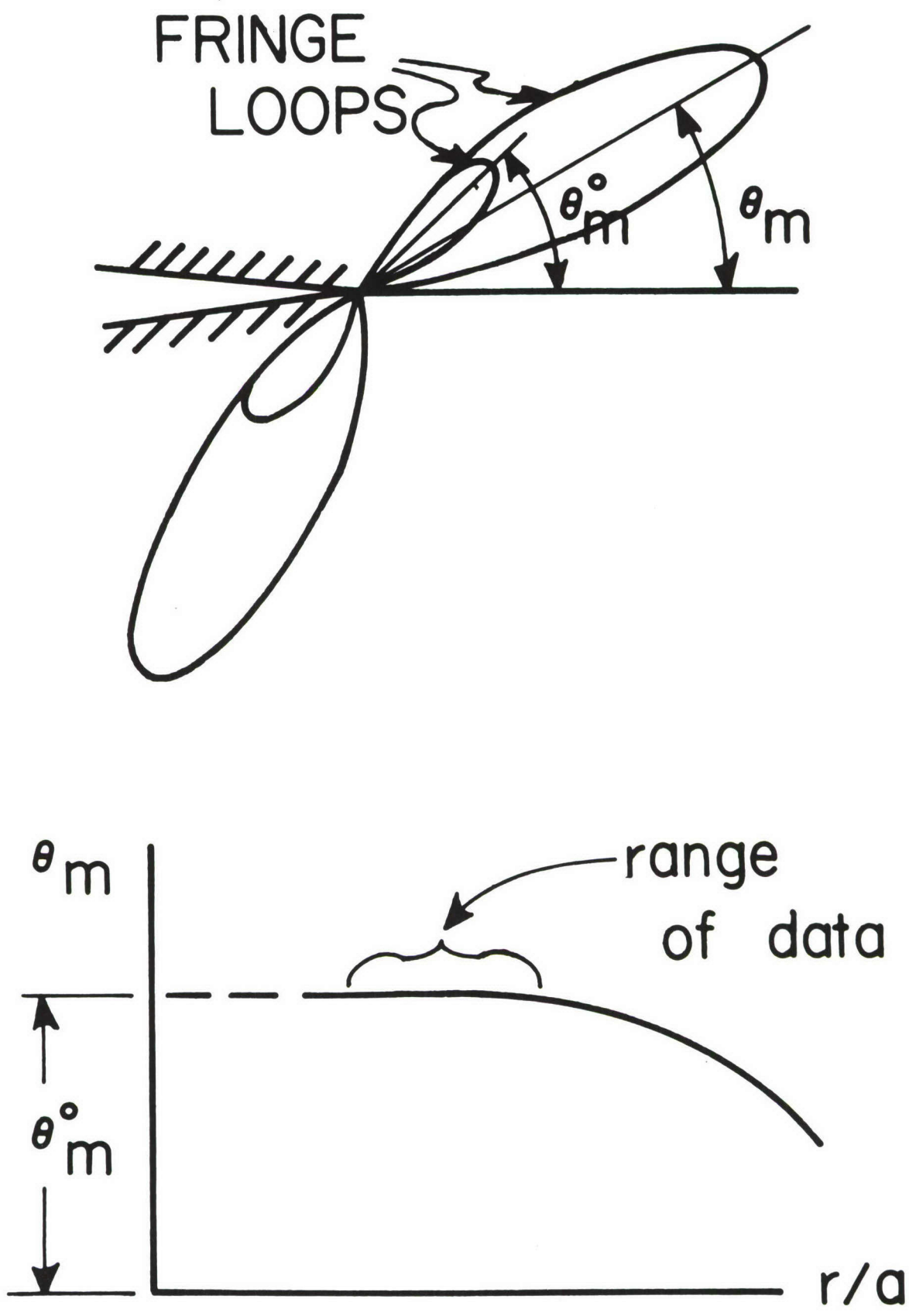

Figure 3) Determination of θ_m^o from Mixed Mode Fringes

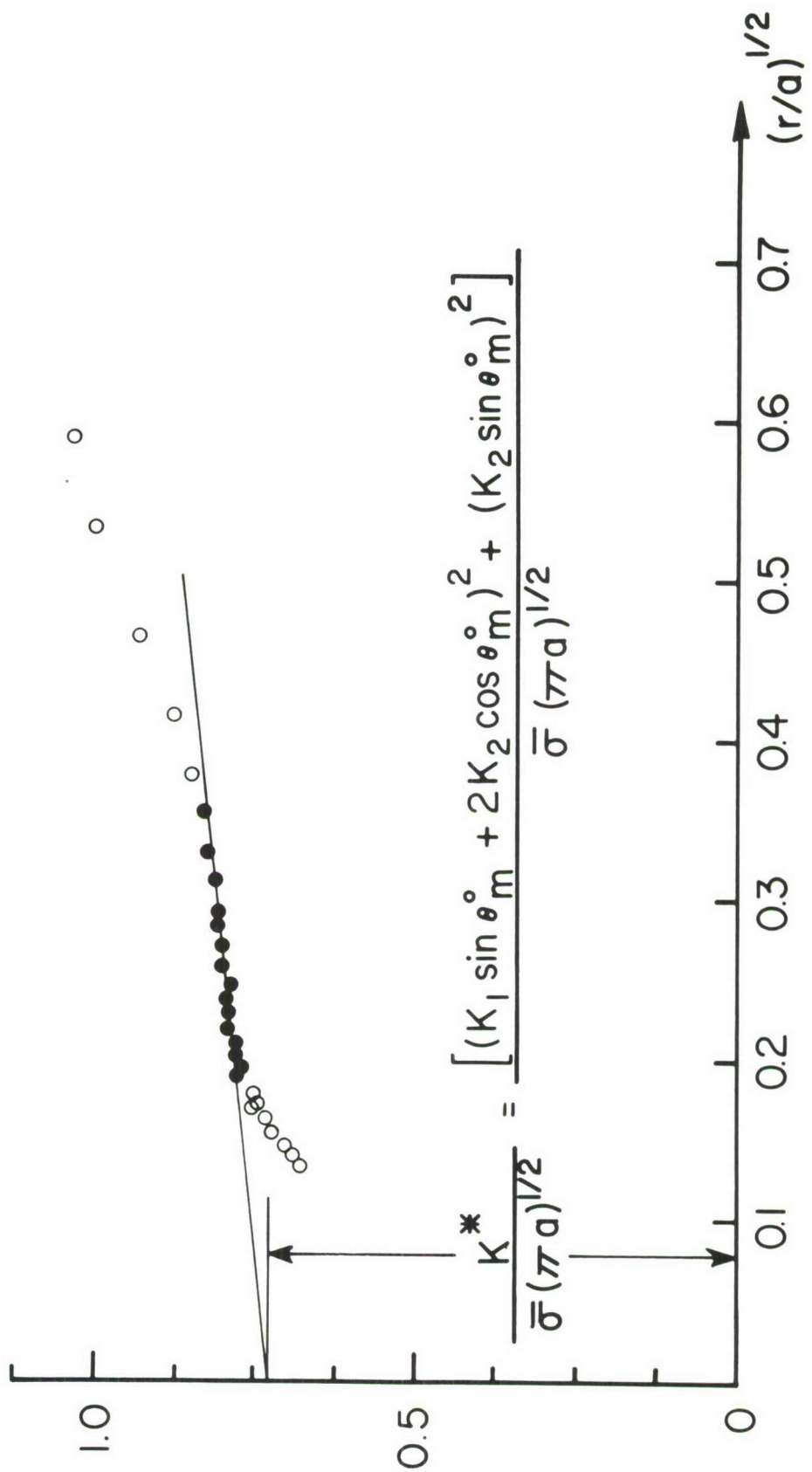

Figure 4) Determination of K* from Typical Slice Data

Figure 5) Kelvin Model

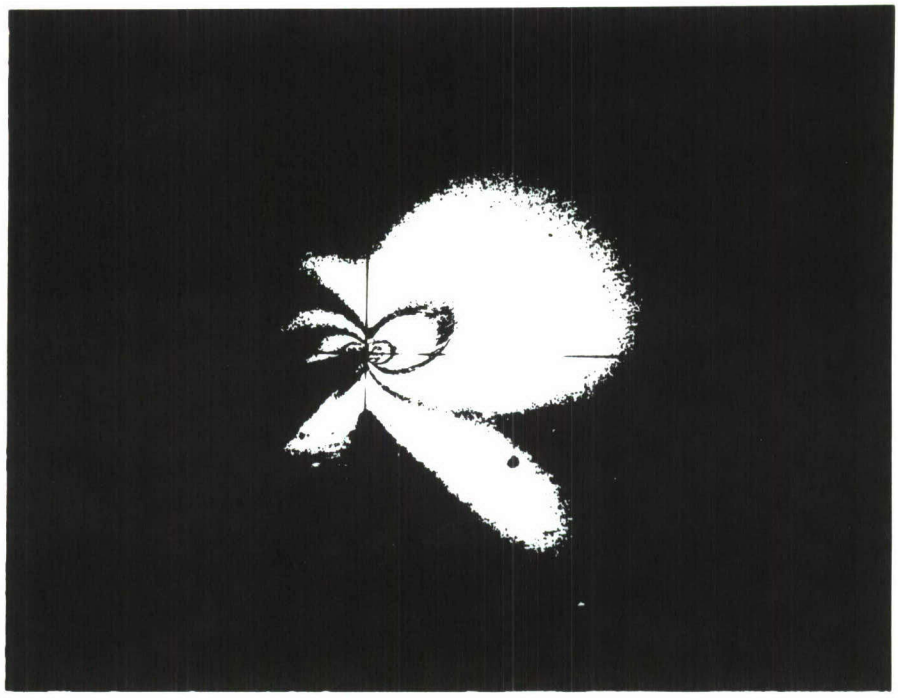

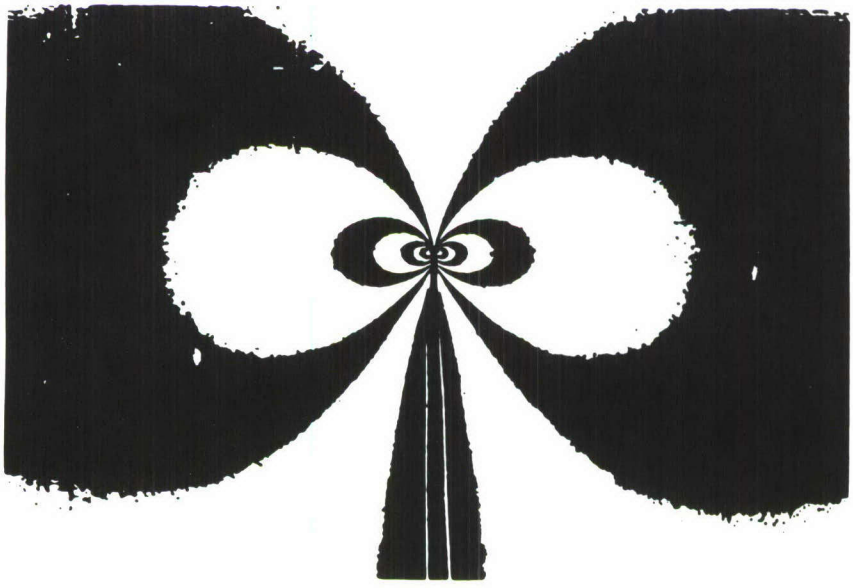

Figure 6) Typcial a) Mixed and b) Mode I fringe patterns

Table I

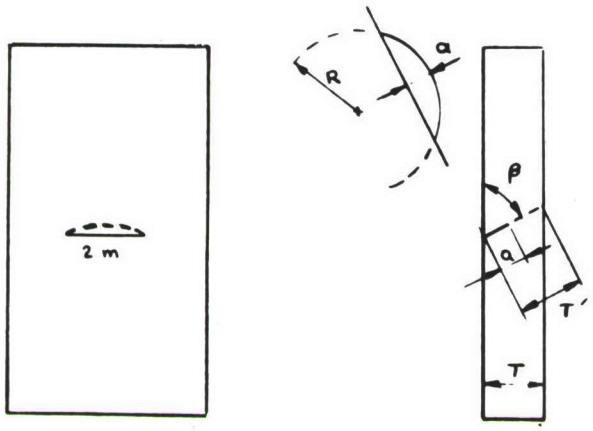

$$T' = \frac{T}{\sin \beta}$$

$$\bar{K}_1 = \bar{\sigma} \sin^2\beta(\pi a)^{1/2}$$

$$\bar{K}_2 = \bar{\sigma} \sin \beta \cos \beta(\pi a)^{1/2}$$

Test No.	β	a(mm)	2R(mm)	2m(mm)	T(mm)	T'(mm)	a/2m	a/T'	α_{max}°	Notch Width(mm)	$\bar{\sigma}$(kpa)
1	30°	5.49	76.2	39.37	13.67	27.43	0.139	0.200	31.11	0.889	103.10
2	30°	6.09	38.1	27.94	13.72	27.43	0.218	0.222	47.17	0.533	102.30
3	60°	4.32	101.6	40.99	13.46	15.54	0.105	0.278	23.79	1.372	76.76
4*	60°	4.32	25.4	19.08	12.78	14.76	0.226	0.293	48.70	0.432	80.28
5	30°	9.53	101.6	59.18	13.59	27.18	0.161	0.350	35.66	1.372	93.72
6	30°	10.89	76.2	53.34	13.46	26.90	0.204	0.405	44.43	0.889	104.10
7	60°	7.26	50.8	35.56	12.75	14.73	0.204	0.493	44.43	0.940	81.03
8	60°	7.62	101.6	53.52	13.64	15.75	0.142	0.484	31.79	1.372	75.72
9	30°	9.53	76.2	50.29	7.32	14.63	0.189	0.650	41.40	0.889	63.45
10	30°	9.53	50.8	33.05	7.29	14.58	0.288	0.653	51.31	0.940	66.07
11	60°	10.99	76.2	53.57	14.17	16.38	0.205	0.672	44.66	0.889	72.28
12	60°	10.16	50.8	40.64	12.45	14.38	0.250	0.707	53.13	0.940	83.03
13	30°	17.60	203.2	114.30	14.05	28.09	0.154	0.627	34.23	3.429	72.90
14	30°	18.69	101.6	78.74	14.30	28.60	0.237	0.654	50.81	1.372	71.59
15[a]	90°	6.35	76.2	42.11	12.70	12.70	0.151	0.500	33.56	0.889	66.10
16[b]	90°	6.35	76.2	42.11	12.45	12.45	0.151	0.510	33.56	0.889	67.74

*** Avg. of 4 experiments**

All plates are 178 mm wide except

a - plate width = 137.8 mm

b - plate width = 117.2 mm

Test Geometries for Figures 7-22

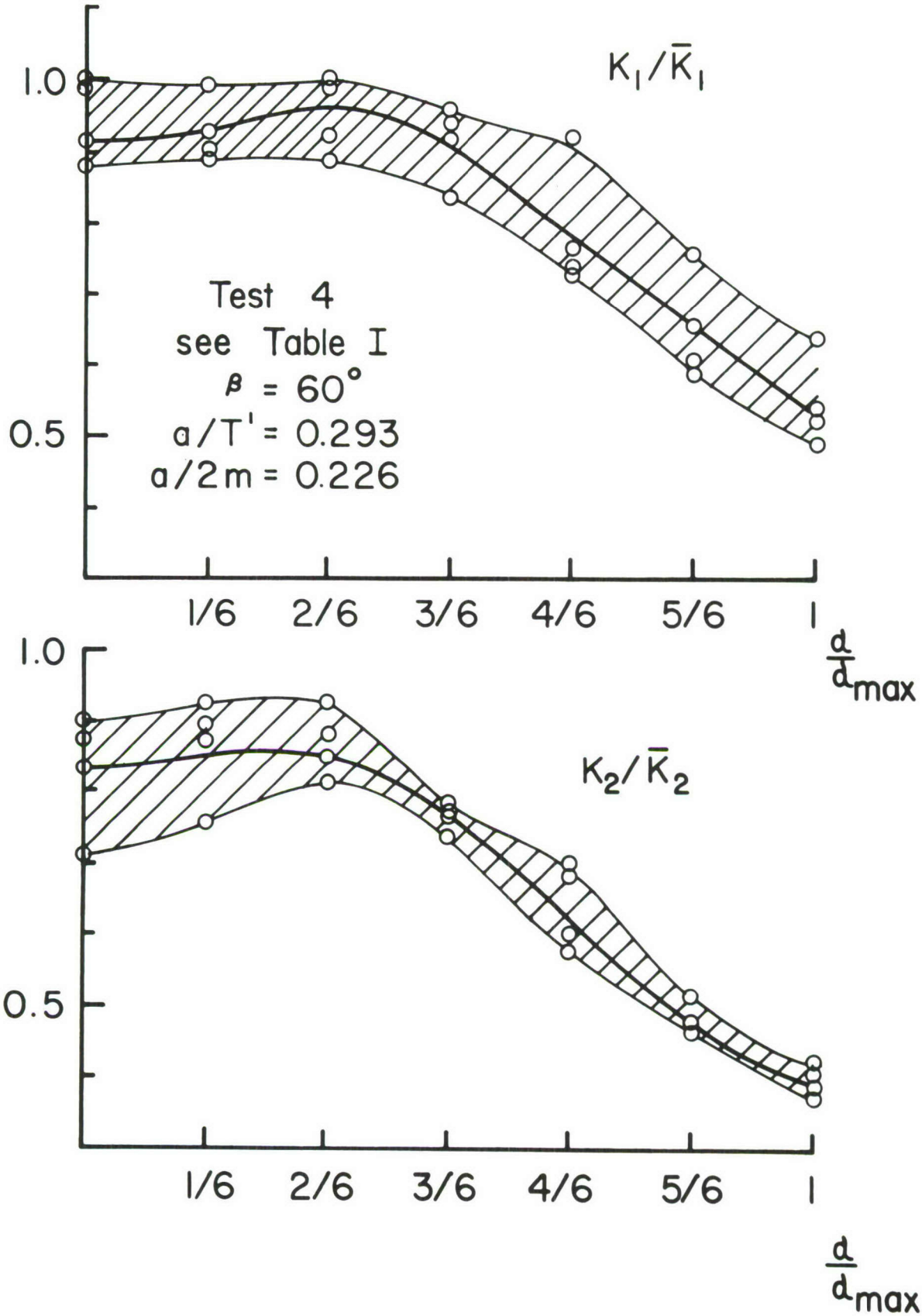

Figure 7) Mixed Mode SIF Distributions for Tests 4

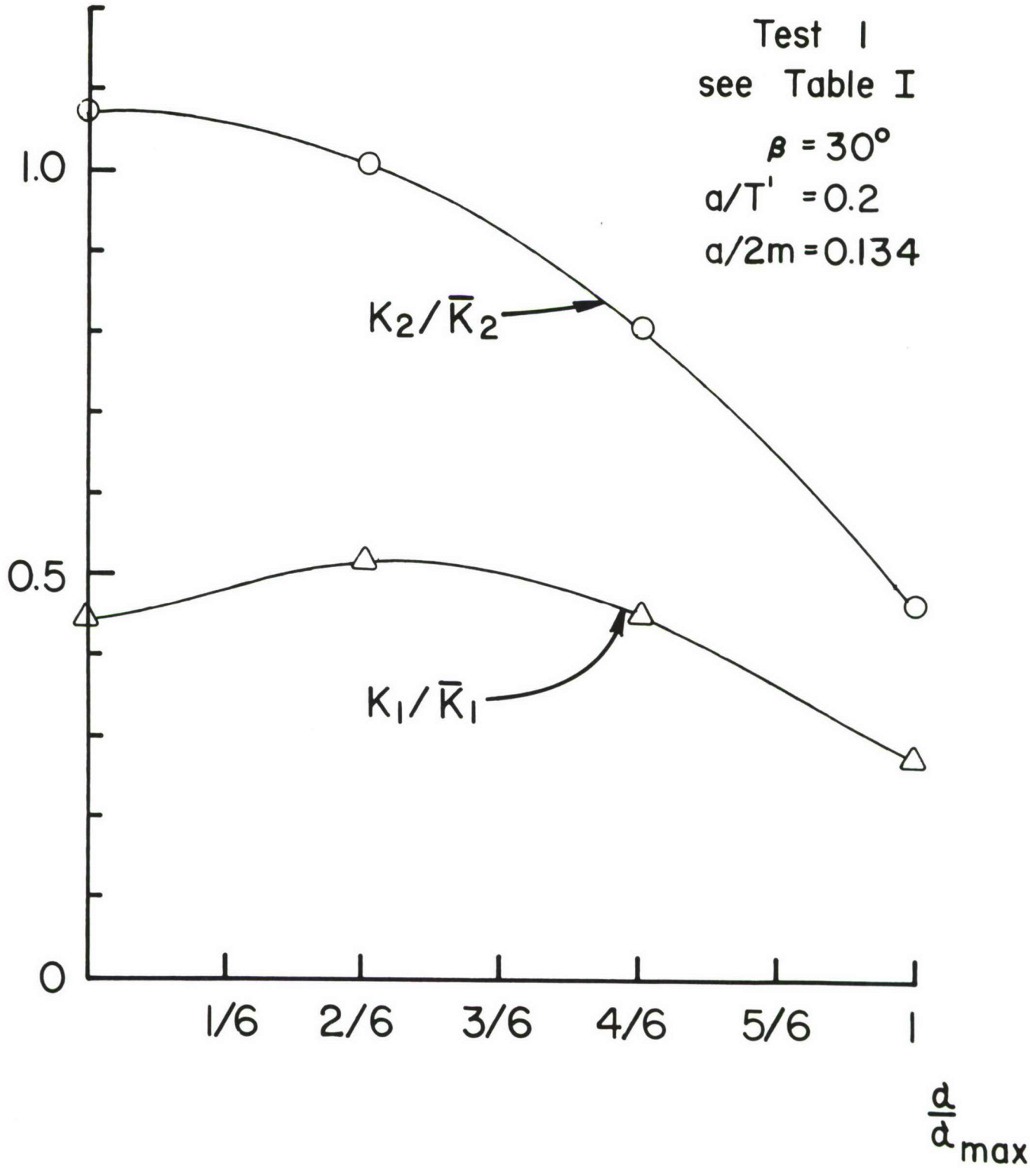

Figure 8) Mixed Mode SIF Distributions for Test 1

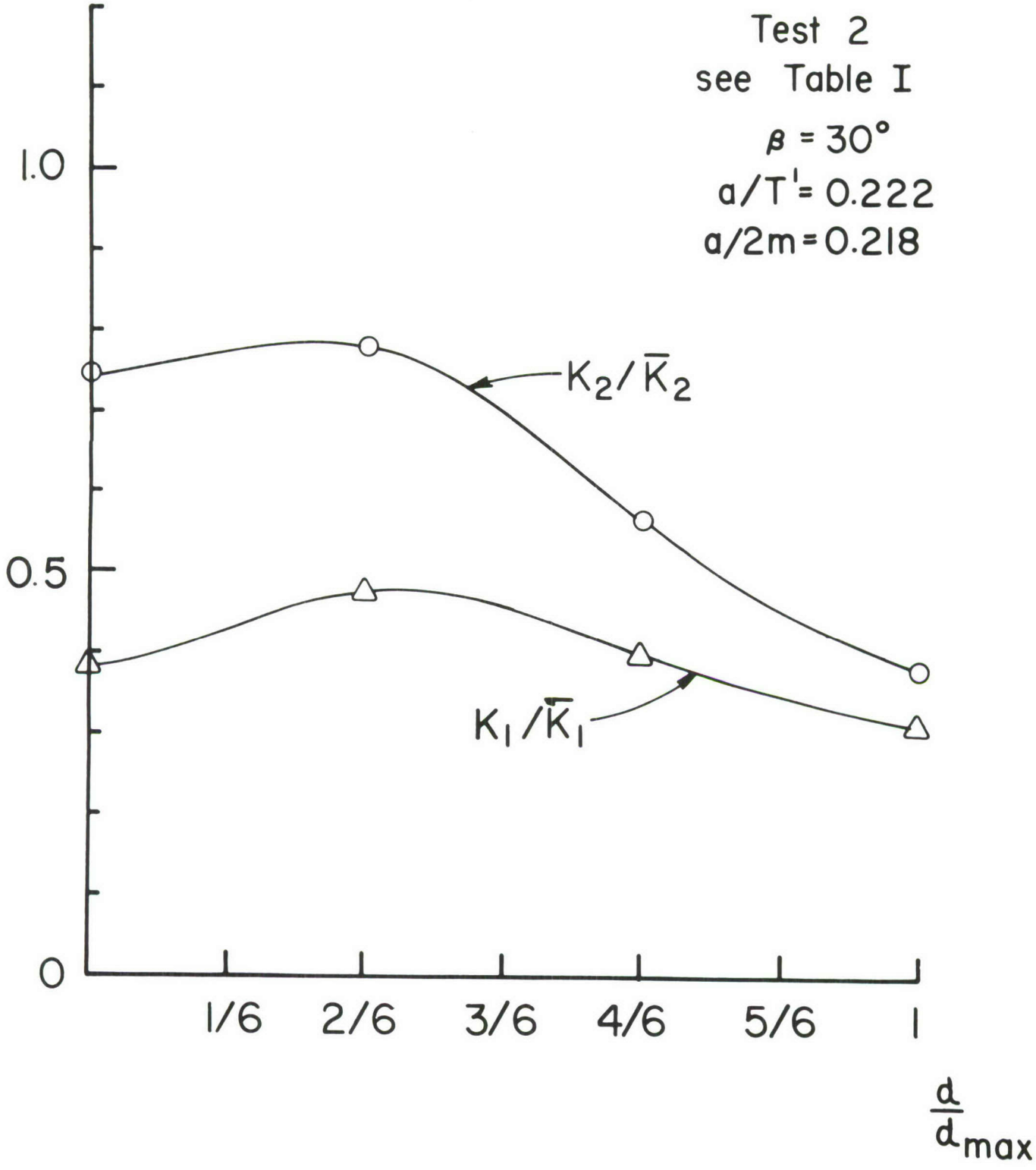

Figure 9) Mixed Mode SIF Distributions for Test 2

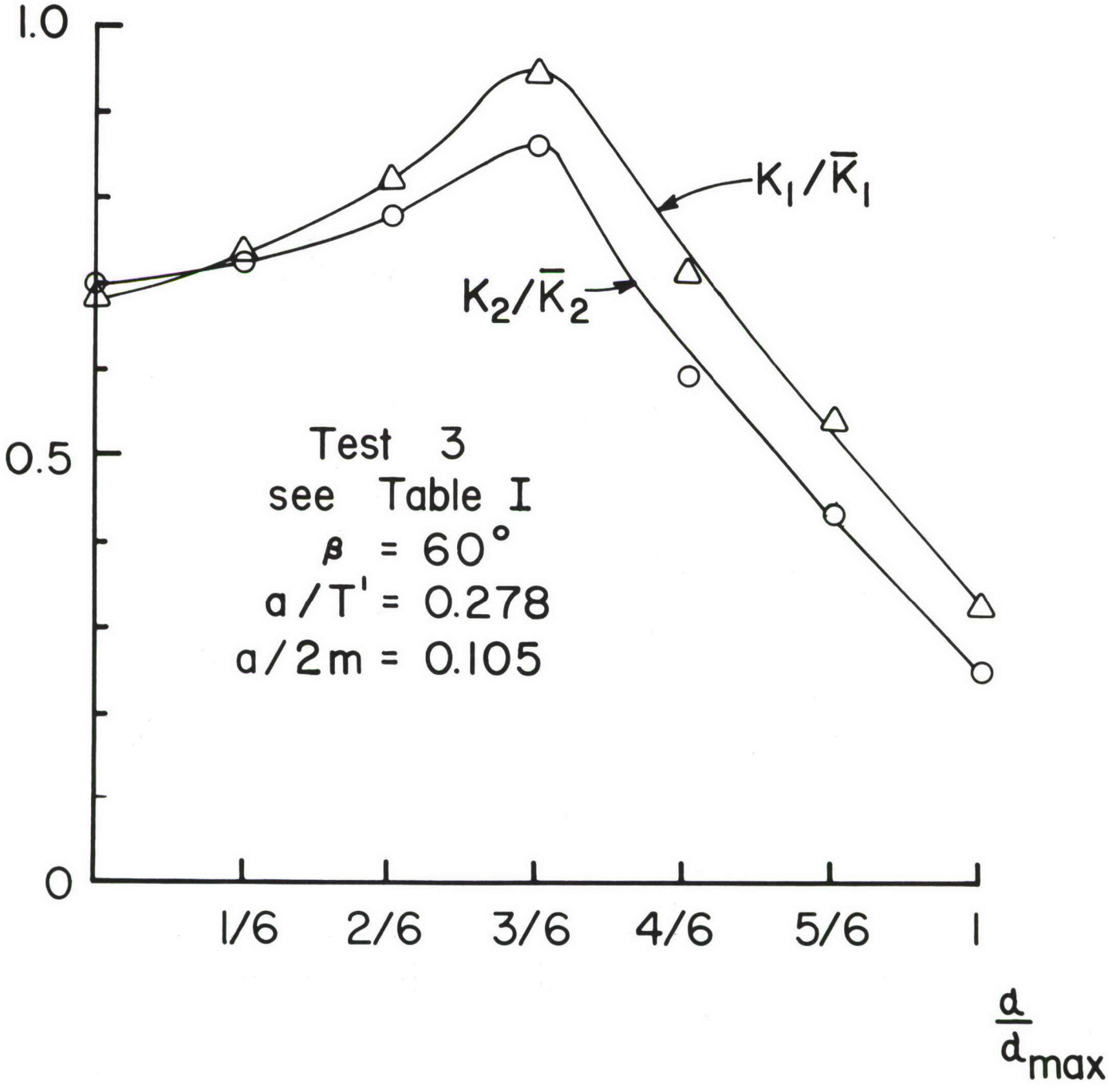

Figure 10) Mixed Mode Distributions for Test 3

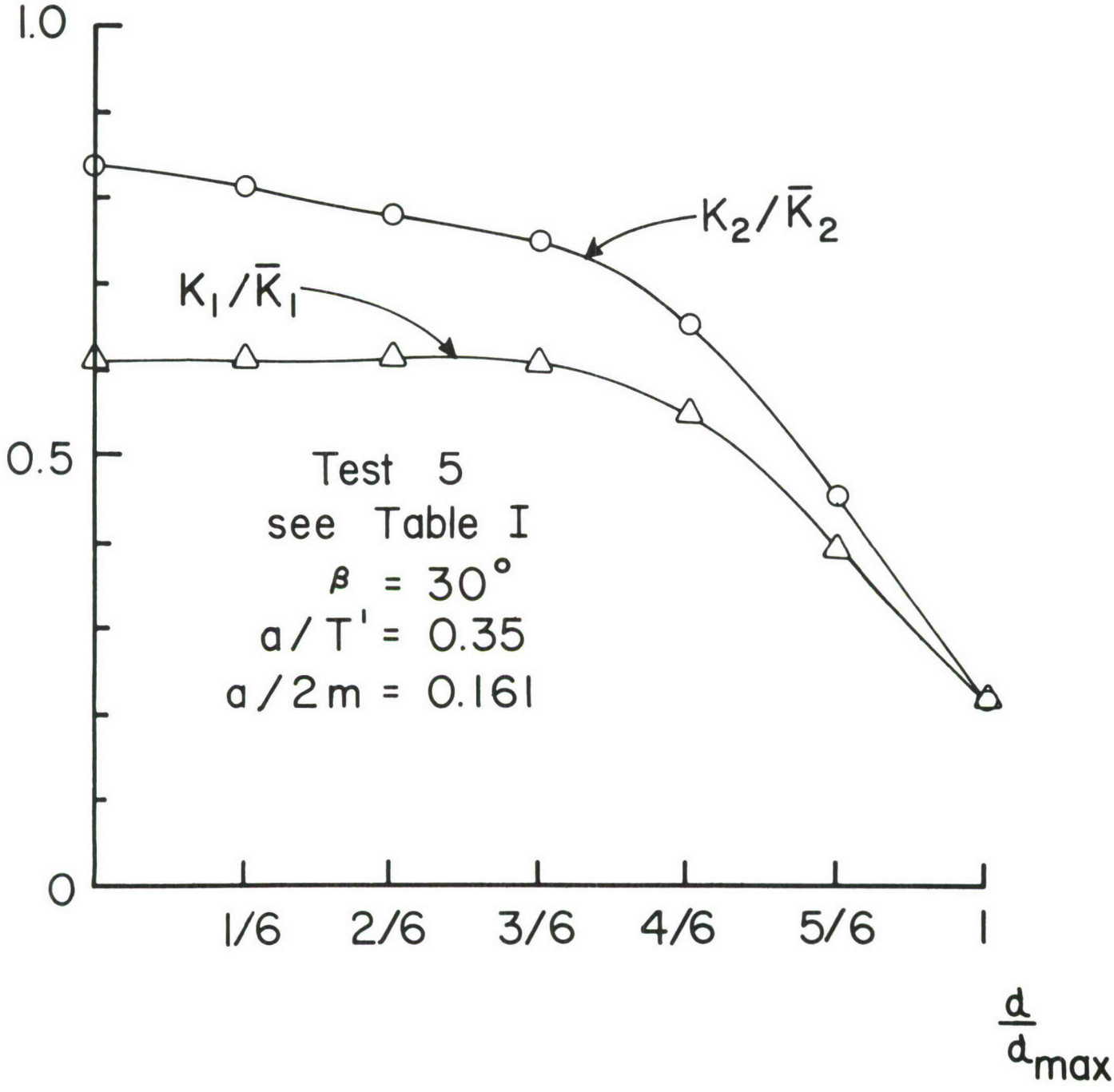

Figure 11) Mixed Mode SIF Distributions for Test 5

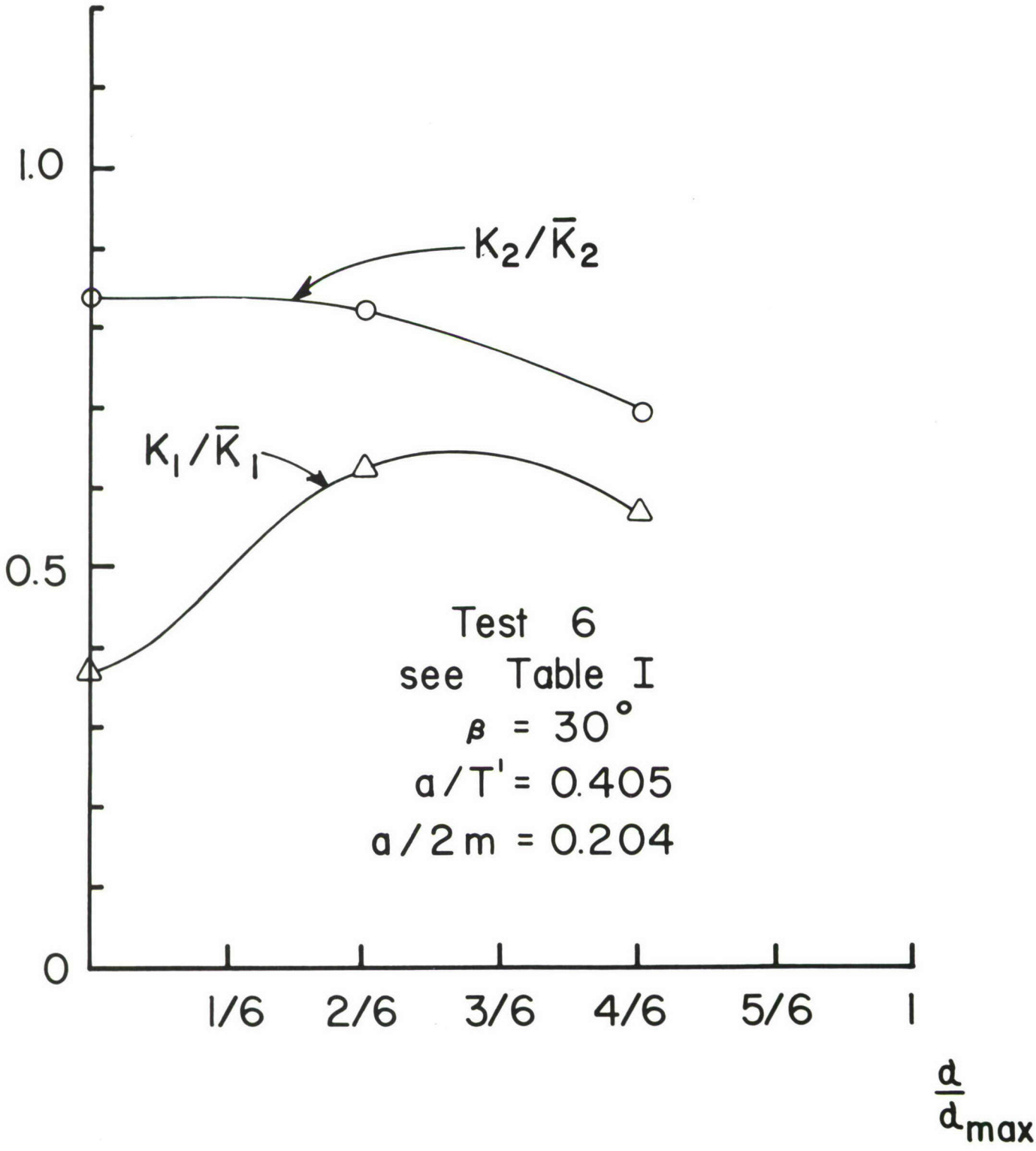

Figure 12) Mixed Mode SIF Distributions for Test 6

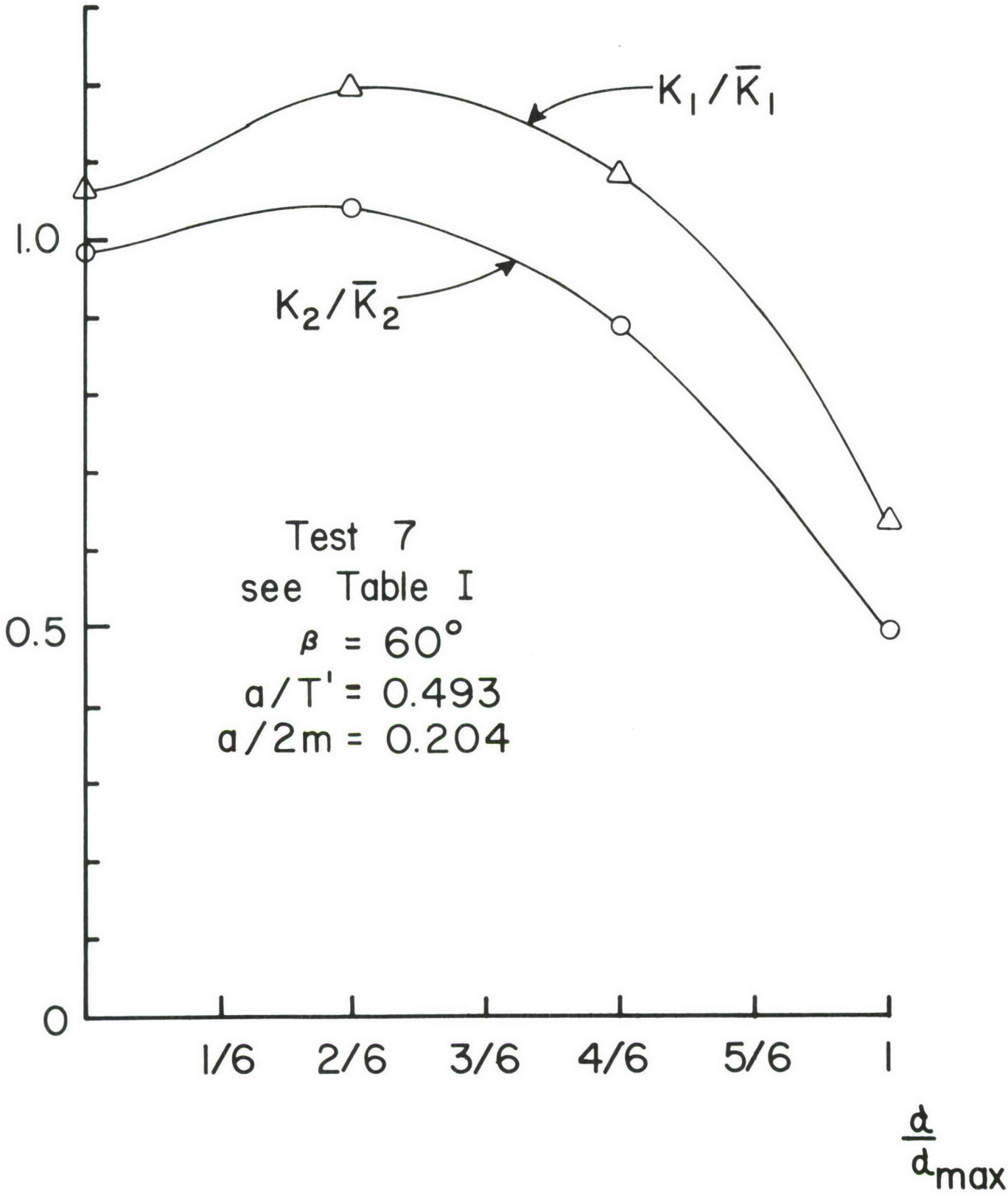

Figure 13) Mixed Mode SIF Distributions for Test 7

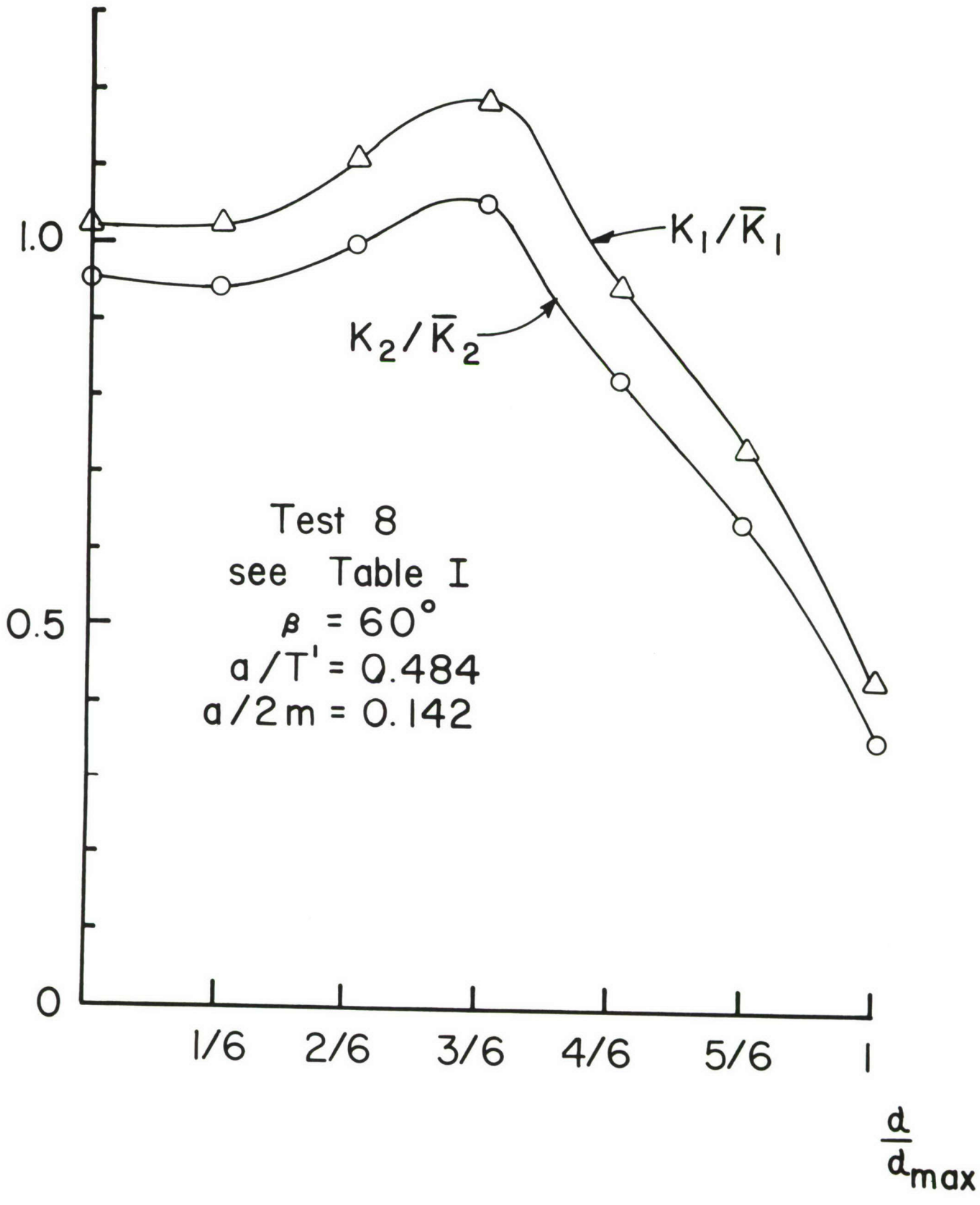

Figure 14) Mixed Mode SIF Distributions for Test 8

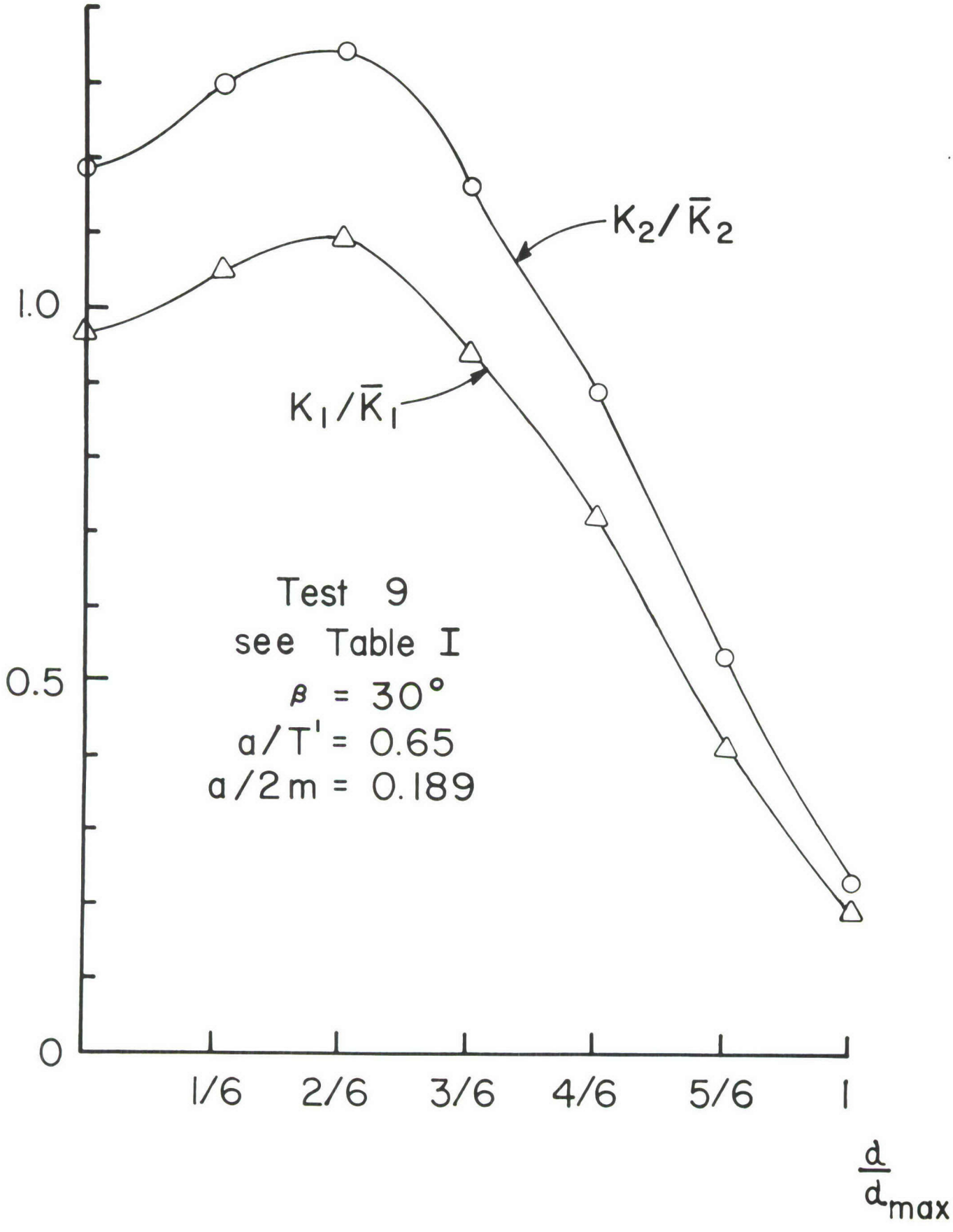

Figure 15) Mixed Mode SIF Distributions for Test 9

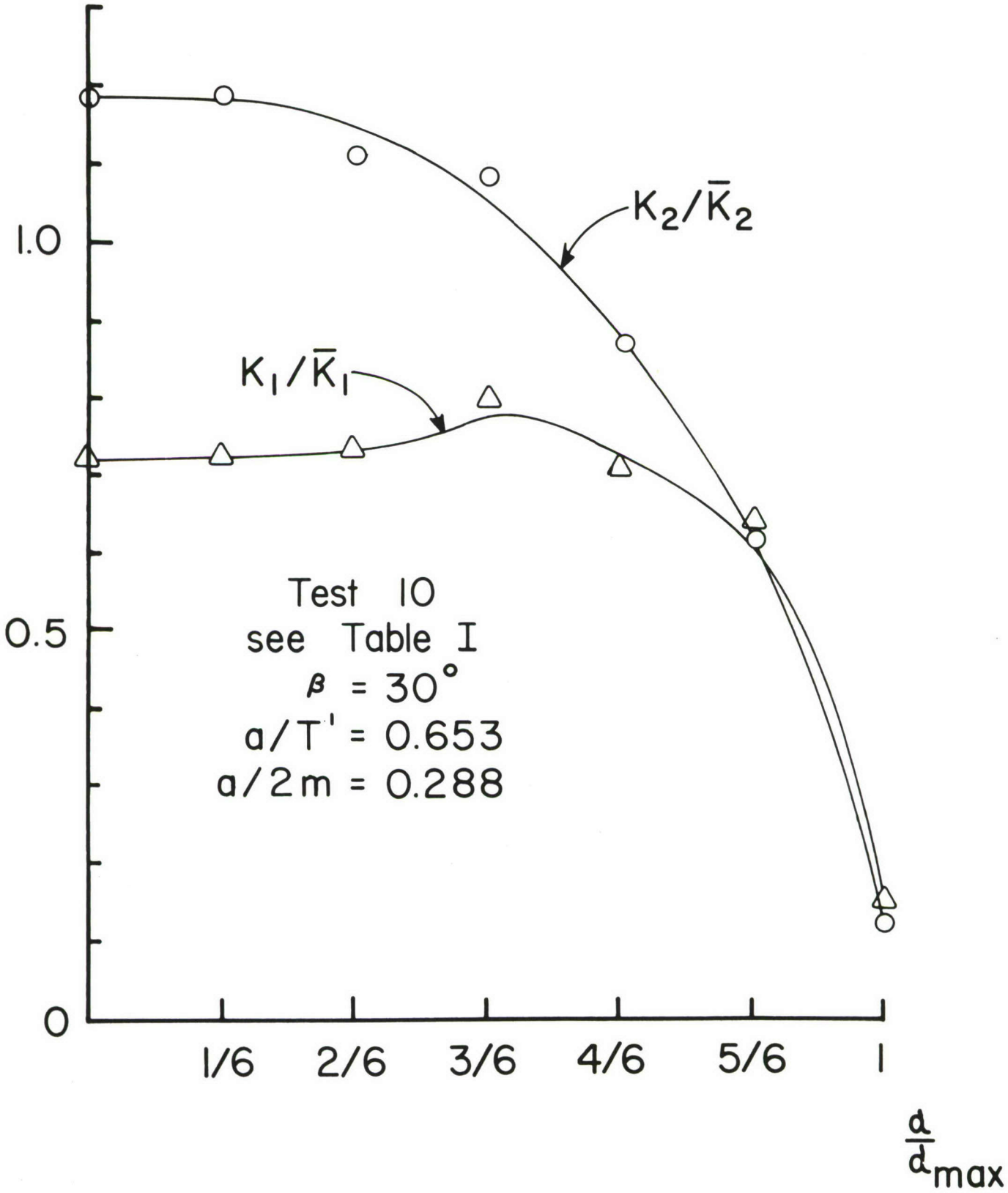

Figure 16) Mixed Mode SIF Distributions for Test 10

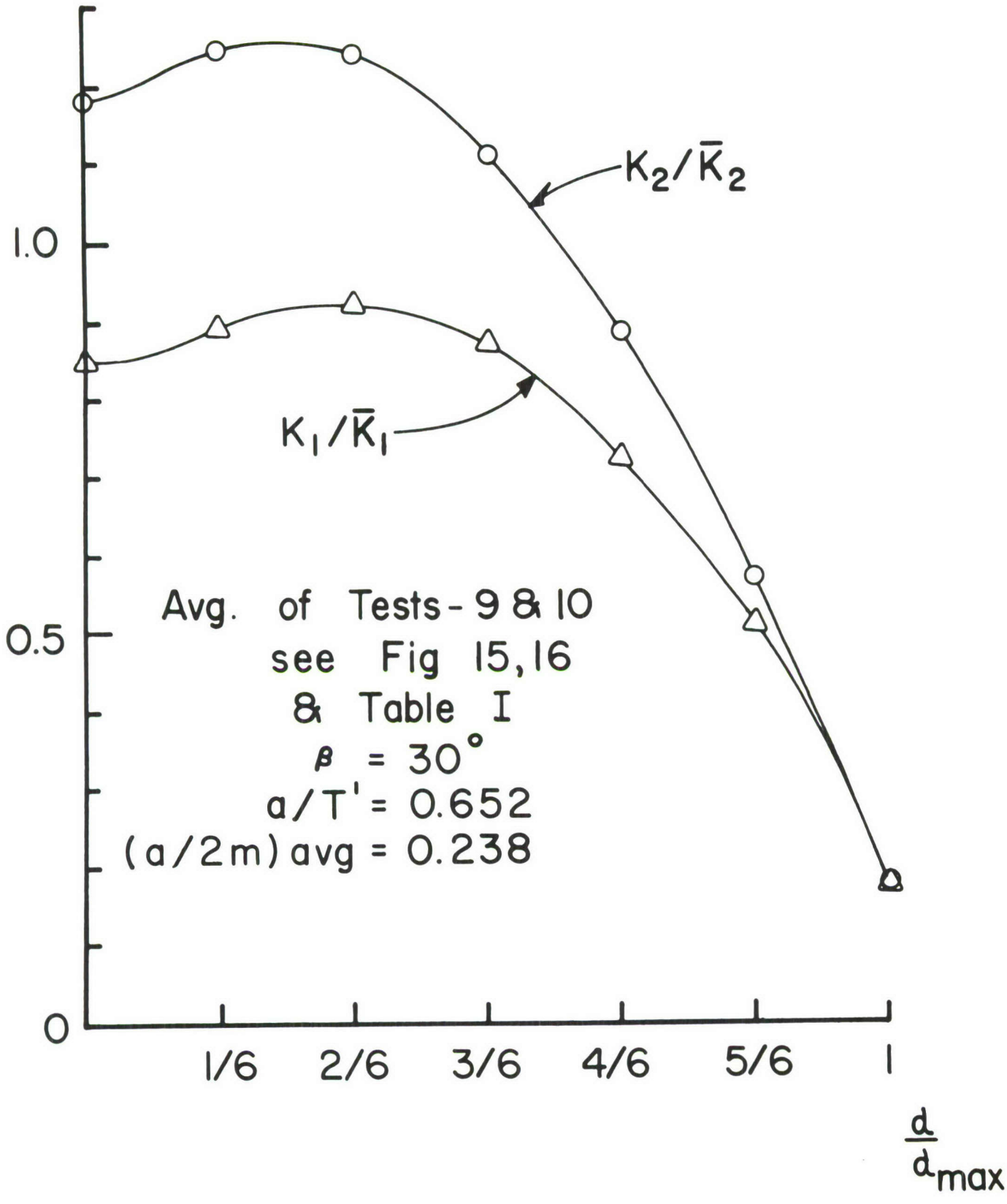

Figure 17) Mixed Mode SIF Distributions for Avg. Tests 9, 10

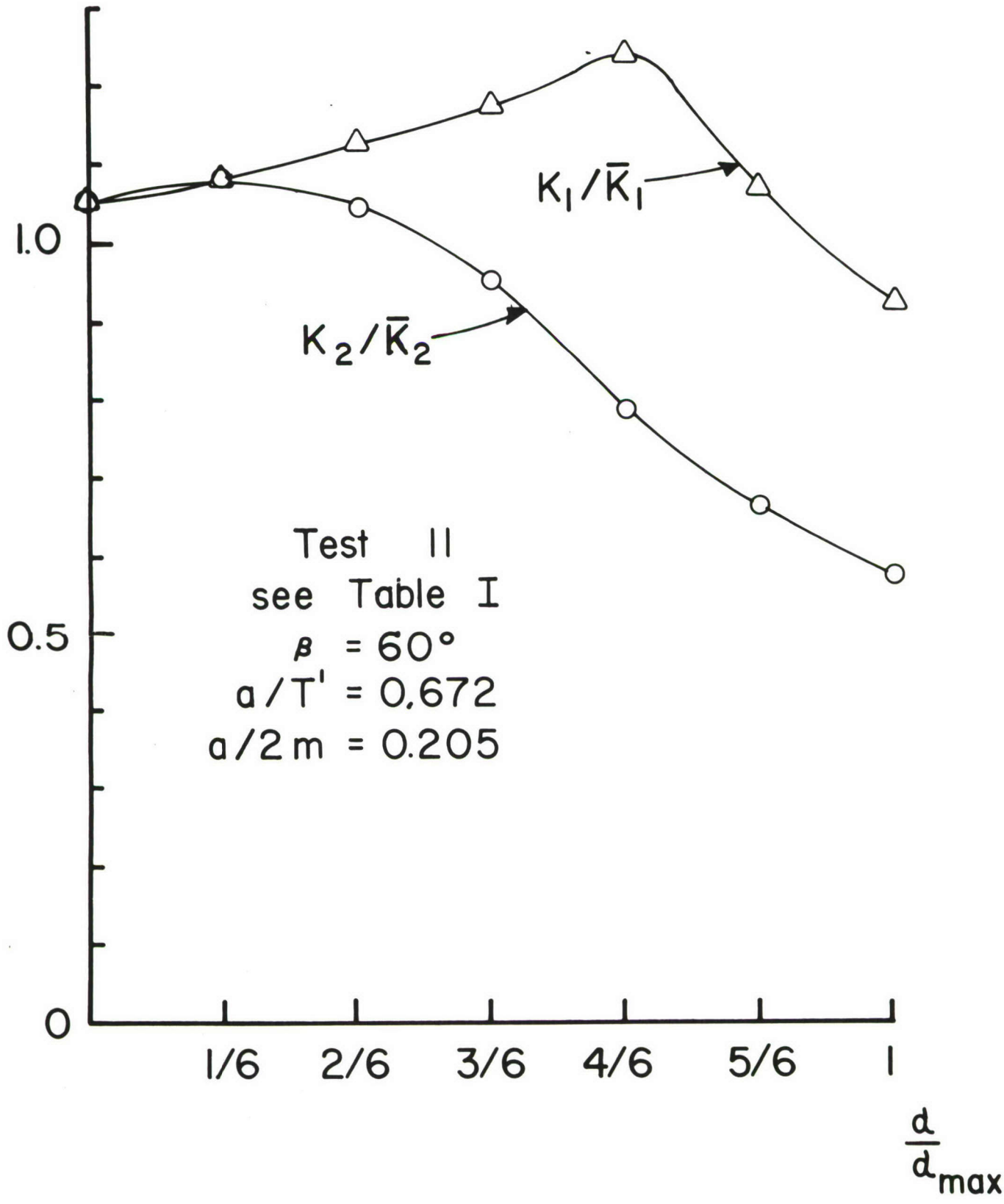

Figure 18) Mixed Mode SIF Distributions for Test 11

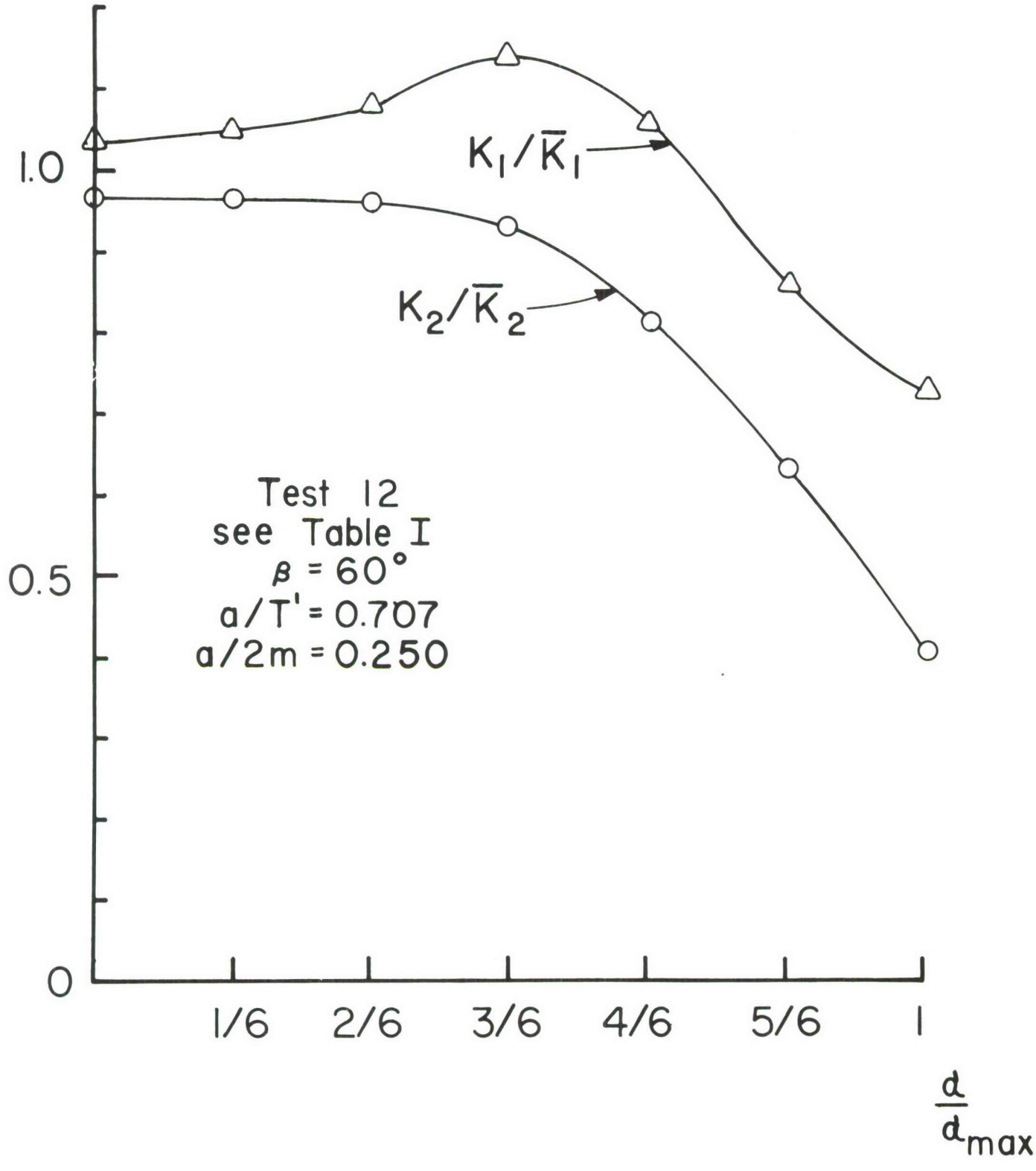

Figure 19) Mixed Mode SIF Distributions for Test 12

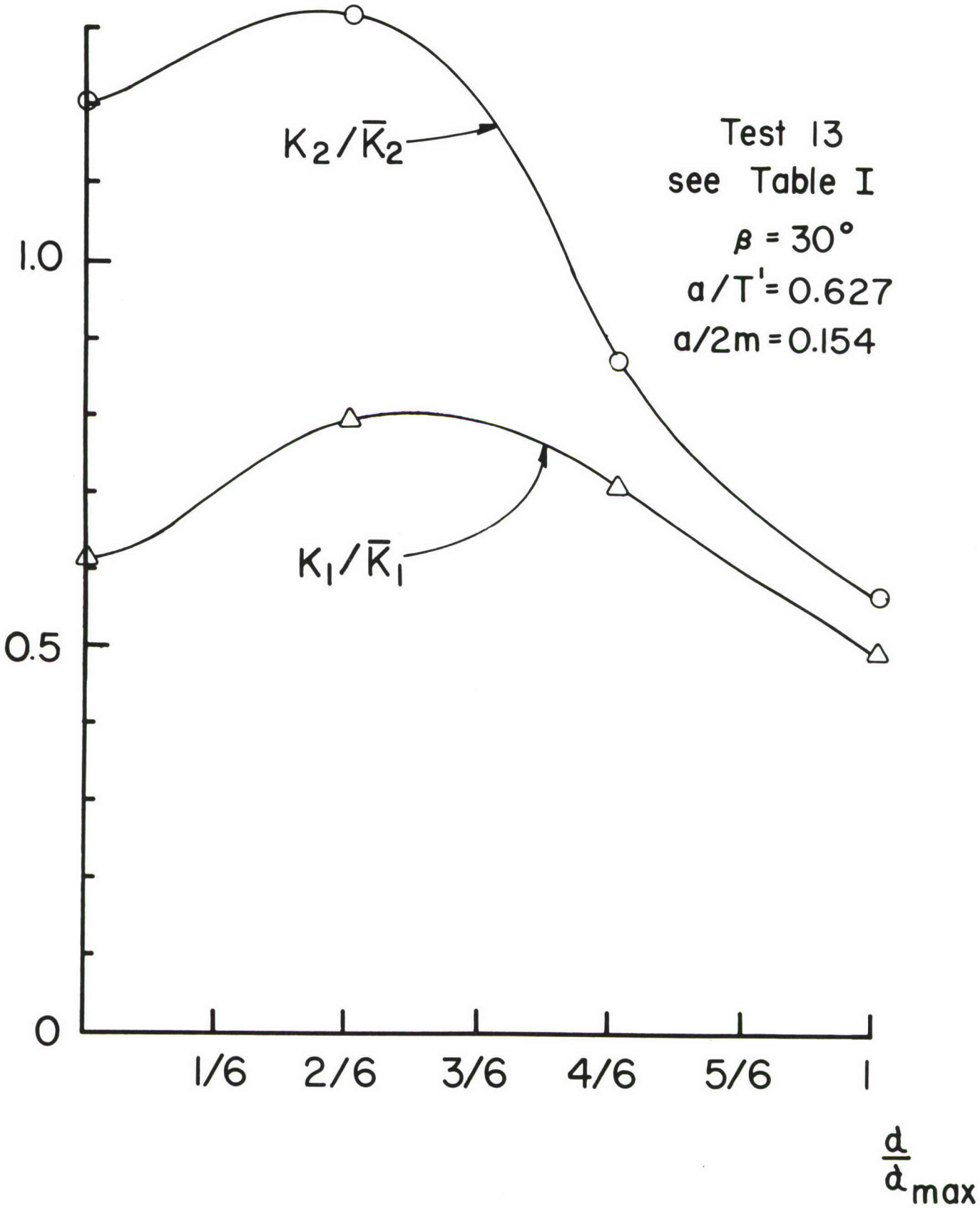

Figure 20) Mixed Mode SIF Distributions for Test 13

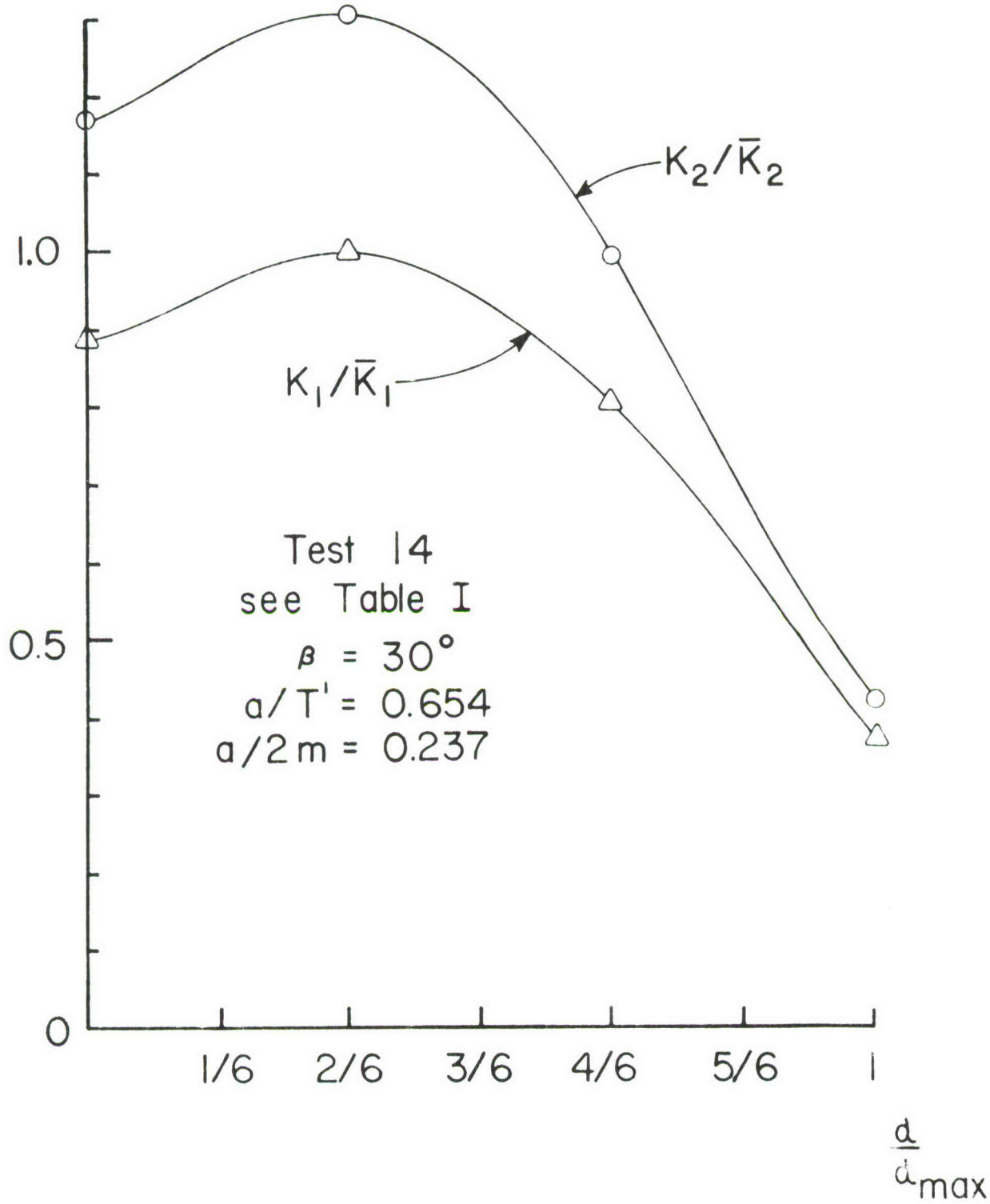

Figure 21) Mixed Mode SIF Distributions for Test 14

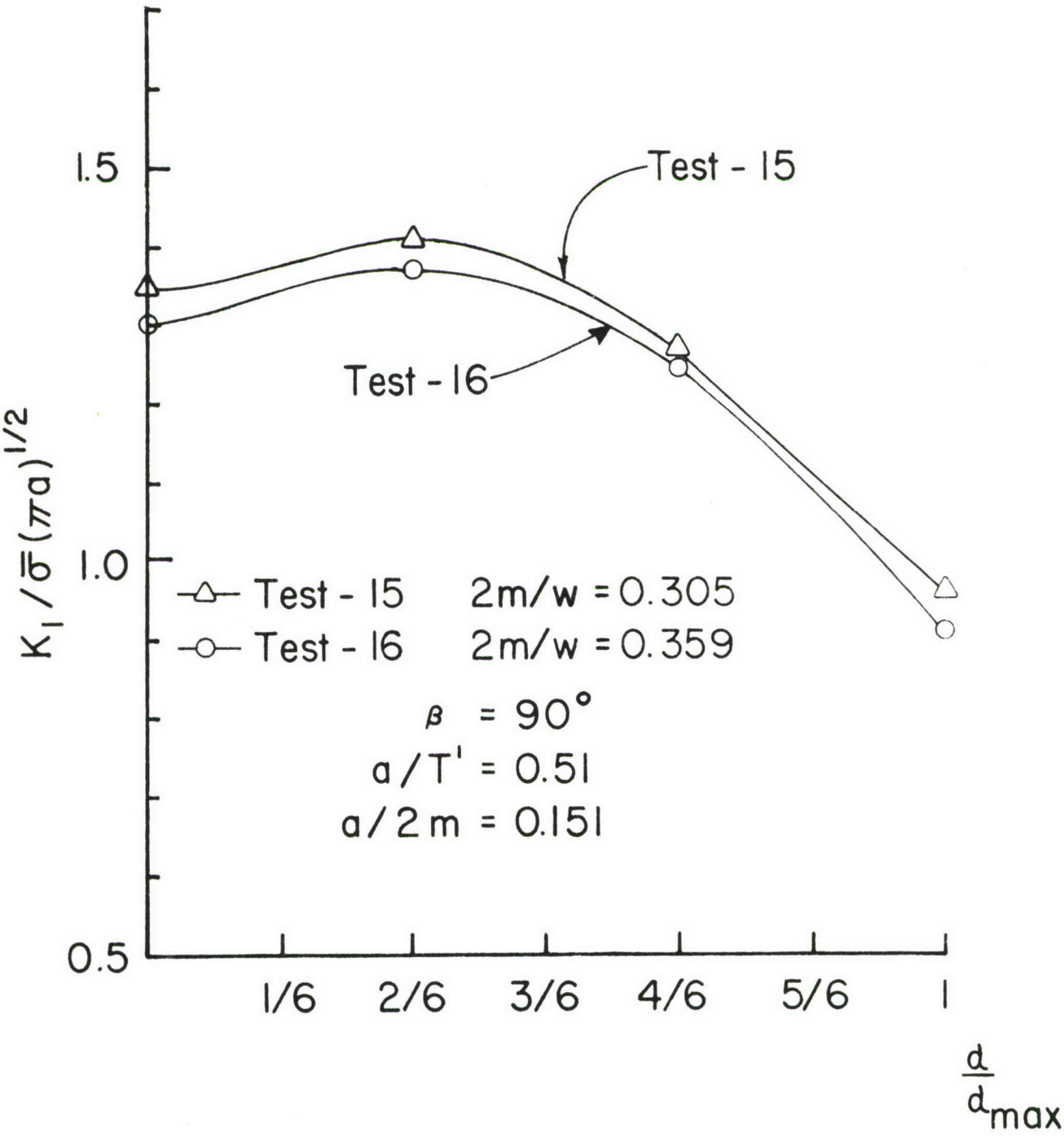

Figure 22) Mixed Mode SIF Distributions for Test 15, 16

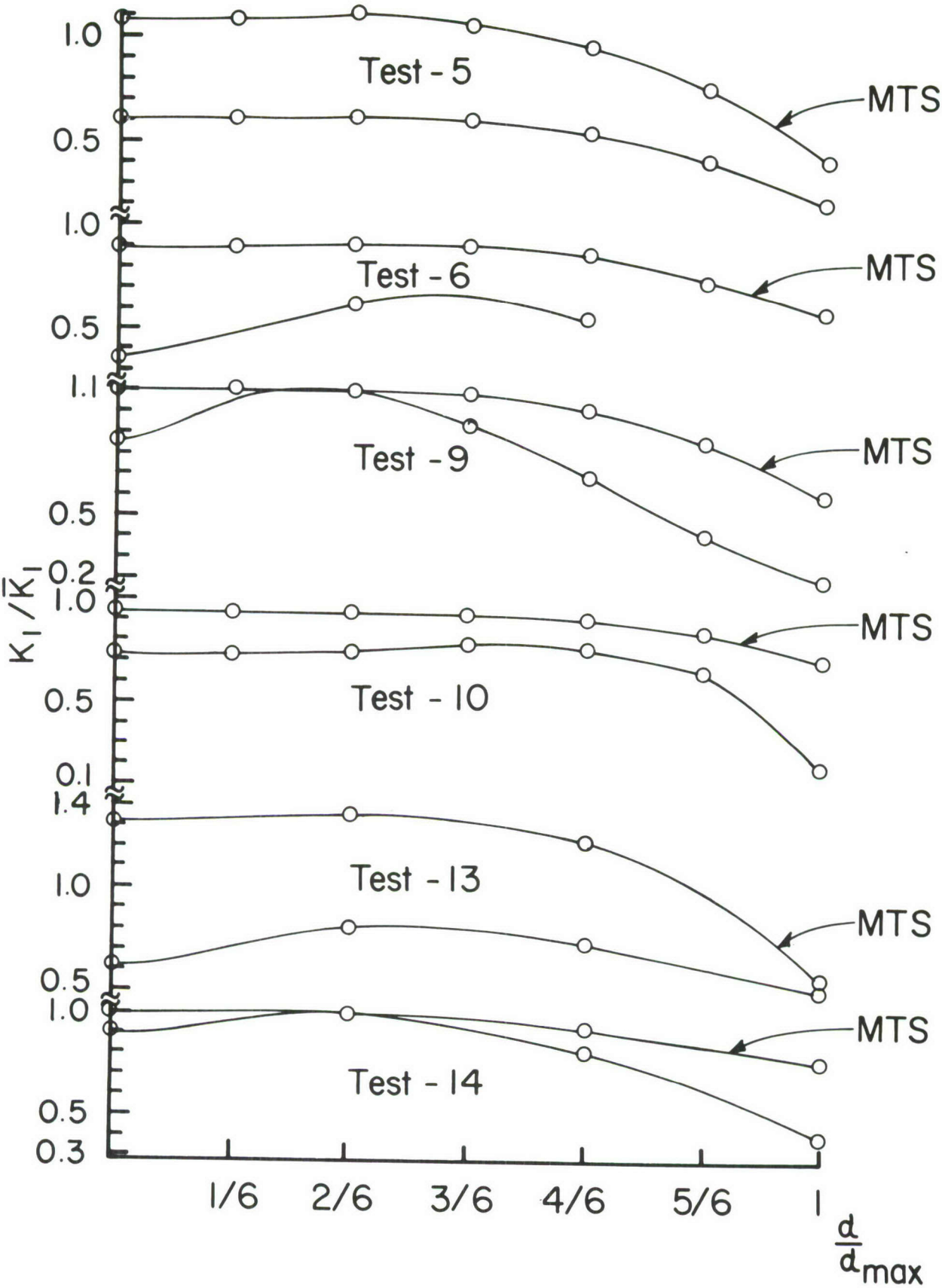

Figure 23) Comparison of Mode I Results with Modified Thresher-Smith (MTS) Theory ($\beta = 30°$)

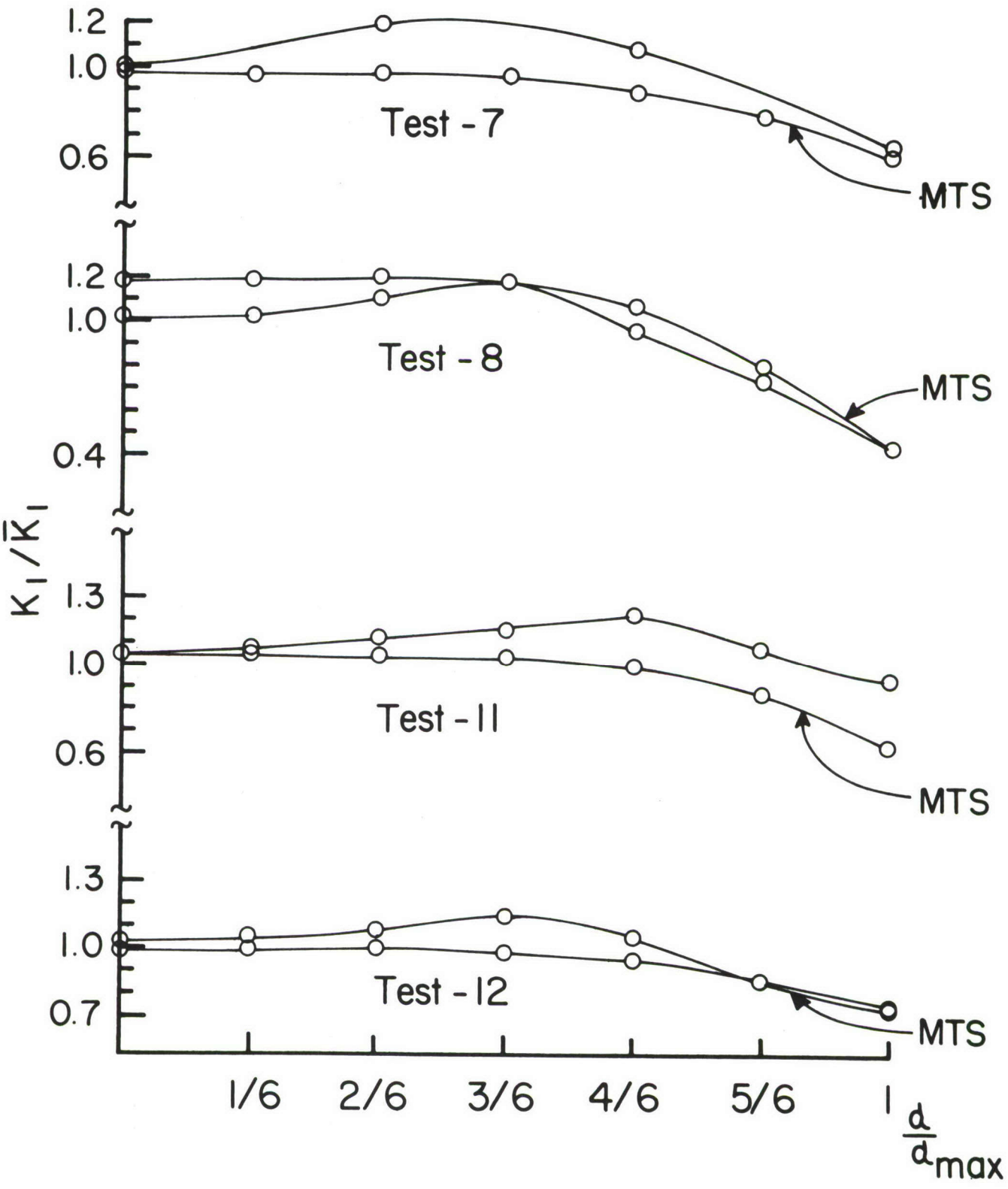

Figure 24) Comparison of Mode I Results with Modified Thresher-Smith (MTS) Theory ($\beta = 60°$)

REFERENCES

1. Irwin, G. R., "The Crack Extension Force for a Part Through Crack in a Plate", Journal of Applied Mechanics, Vol. 29, Trans. ASME, Vol. 79, Series E, Dec. 1962, pp. 651-654.

2. Swedlow, J. L., Ed., The Surface Crack: Physical Problems and Computational Solutions, Symposium Proceedings ASME Committee for Computing in Applied Mechanics of AMD, Nov. 1972.

3. Rybicki, E. F. and Benzley, S. E., Eds., Computational Fracture Mechanics, Symposium Proceedings ASME Computer Technology Committee of Pressure Vessels and Piping Division, June 1975.

4. Anon., Proceedings of a Symposium on Part Through Crack Life Prediction (In Press), ASTM STP, Oct. 1977.

5. Smith, D. G. and Smith, C. W., "A Photoelastic Investigation of Closure and Other Effects Upon Local Bending Stresses in Cracked Plates", International Journal of Fracture Mechanics, Vol. 6, No. 3, Sept. 1970, pp. 305-318.

6. Smith, D. G. and Smith, C. W., "Photoelastic Determination of Mixed Mode Stress Intensity Factors", Engineering Fracture Mechanics, Vol. 4, No. 3, 1972, pp. 357-366.

7. Marrs, G. R. and Smith, C. W., "A Study of Local Stresses Near Surface Flaws in Bending Fields", Stress Analysis and Growth of Cracks, ASTM STP 513, 1972, pp. 22-36.

8. Smith, C. W., "Use of Three Dimensional Photoelasticity and Progress in Related Areas", Chapter I, Vol. 2, Experimental Techniques in Fracture Mechanics, Society for Experimental Stress Analysis Monograph No. 2, 1975, pp. 3-58.

9. Jolles, M., McGowan, J. J. and Smith, C. W., "Use of a Hybrid Computer Assisted Photoelastic Technique for Stress Intensity Determination in Three Dimensional Problems", Ref. 3, pp. 83-102.

10. Smith, C. W., McGowan, J. J. and Jolles, M., "Effects of Artificial Cracks and Poisson's Ratio Upon Photoelastic Stress Intensity Determination", Experimental Mechanics, Vol. 16, No. 5, May 1976, pp. 188-193.

11. McGowan, J. J. and Smith, C. W., "A Finite Deformation Analysis of the Near Field Surrounding the Tip of Crack-Like Elliptical Perforations", International Journal of Fracture, Vol. 11, No. 6, Dec. 1975, pp. 977-987.

12. McGowan, J. J. and Smith, C. W., "A Plane Strain Analysis of the the Blunted Crack Tip Using Small Strain Deformation Plasticity Theory", Advances in Engineering Science, Vol. 2, Nov. 1976, pp. 585-594.

13. Schroedl, M. A., McGowan, J. J. and Smith, C. W., "An Assessment of Factors Influencing Data Obtained by the Photoelastic Stress Freezing Technique for Stress Fields Near Crack Tips", Engineering Fracture Mechanics, Vol. 4, 1972, pp. 801-809.

14. Schroedl, M. A. and Smith, C. W., "A Study of Near and Far Field Effects in Photoelastic Stress Intensity Determination", Engineering Fracture Mechanics, Vol. 7, 1975, pp. 341-355.

15. Smith, C. W., "Stress Intensity Estimates by a Computer Assisted Photoelastic Method", (Invited Paper) In Press - Proceedings of the International Conference of Fracture Mechanics and Technology, Hong Kong, March 1977.

16. Schroedl, M. A. and Smith, C. W., "Local Stresses Near Deep Surface Flaws Under Cylindrical Bending Fields", Progress in Flaw Growth and Fracture Toughness Testing, ASTM STP 536, 1973, pp. 45-63.

17. Schroedl, M. A., McGowan, J. J. and Smith, C. W., "Determination of Stress Intensity factors from Photoelastic Data with Application to Surface Flaw Problems", Experimental Mechanics, Vol. 14, No. 10, Oct. 1974, pp. 392-399.

18. Smith, C. W., "Use of Three Dimensional Photoelasticity in Fracture Mechanics", (Invited Paper), Proceedings of the Third International Congress on Experimental Mechanics, 1974, pp. 287-292.

19. Jolles, M., McGowan, J. J. and Smith, C. W., "Experimental Determination of Side Boundary Effects on Stress Intensity Factors in Surface Flaws", Journal of Engineering Materials and Technology, Vol. 97, 1975, pp. 45-51.

20. McGowan, J. J. and Smith, C. W., "Stress Intensities for Deep Cracks Emanating from the Corner Formed by a Hole Intersecting a Plate Surface", Mechanics of Crack Growth, ASTM STP 590, 1976, pp. 460-476.

21. Jolles, M., McGowan, J. J. and Smith, C. W., "Stress Intensities for Cracks Emanating from Holes in Finite Thickness Plates by a Modified Computer Assisted Photoelastic Method", Proceedings of the 12th Annual Meeting of the Society for Engineering Science, 1975, pp. 352-362.

22. Harms, A. E. and Smith, C. W,, "Stress Intensity Factors for Long, Deep Surface Flaws in Plates Under Extensional Fields", Recent Advances in Engineering Science, Vol. 7, 1976, pp. 59-66.

23. Smith, C. W. and Jolles, M., "Stress Intensities in Deep Surface Flaws in Plates Under Mode I Loading", Developments in Theoretical and Applied Mechanics, Vol. 8, 1975, pp. 151-160.

24. Smith, C. W., Jolles, M. and Peters, W. H., "Stress Intensities for Cracks Emanating from Pin-Loaded Holes", Flaw Growth and Fracture, ASTM STP 631, 1977, pp. 190-201.

25. Smith, C. W., Jolles, M. and Peters, W. H., "Stress Intensities in Flawed Pressure Vessels", Proceedings of the Third International Conference on Pressure Vessel Technology, Part II - Materials and Fabrication, ASME, April 1977, pp. 535-543.

26. Smith, C. W., Jolles, M. and Peters, W. H., "An Experimental Study of the Plate-Nozzle Tensile Test for Cracked Reactor Vessel Nozzles", Developments in Mechanics, Vol. 8, March 1977, pp. 29-31.

27. Smith, C. W., Jolles, M. I. and Peters, W. H., "Geometric Influences Upon Stress Intensity Distributions along Reactor Vessel Nozzle Cracks", Paper G 4/3, Transactions of the 4th International Conference on Structural Mechanics in Reactor Technology, Aug. 1977, 8 pp.

28. Smith, C. W., Jolles, M. I. and Peters, W. H., "Stress Intensities for Nozzle Cracks in Reactor Vessels" (In Press), Experimental Mechanics, Vol. 17, No. 12, Dec. 1977.

29. Smith, C. W. and Peters, W. H., "Use of the Frozen Stress Method in the Stress Analysis of Flawed Bodies", Recent Advances in Engineering Science, Vol. 14, 1977, pp. 991-999.

30. Smith, C. W., Peters, W. H. and Jolles, M. I., "Stress Intensity Factors for Reactor Vessel Nozzle Cracks", Invited Paper No. 77-PVP-30 (In Press), Journal of Pressure Vessel Technology, 13 pp.

31. Smith, F. W. and Sorensen, D. R., "Mixed Mode Stress Intensity Factors for Semi-Elliptical Surface Cracks", NASA CR-134684, 1974, 97 pp.

32. Kassir, M. and Sih, G. C., "Three Dimensional Stress Distribution Around an Elliptical Crack Under Arbitrary Loading", Journal of Applied Mechanics, Vol. 33, No. 3, Sept. 1966, pp. 601-611.

33. Sneddon, I. N., "The Distribution of Stress in the Neighborhood of a Crack in an Elastic Solid", Proceedings of the Royal Society, Series A, Vol. 187, 1964, pp. 229-260.

34. Thresher, R. W. and Smith, F. W., "Stress Intensity Factors for a Surface Crack in a Finite Solid", Journal of Applied Mechanics, Series E, Vol. 39, No. 1, March 1972, pp. 195-200.

35. Gross, B. and Mendelson, A., "Plane Elastostatic Analysis of V-Notched Plates", International Journal of Fracture Mechanics, Vol. 8, No. 3, Sept. 1972, pp. 267-276.

36. Wells, A. and Post, D., "The Dynamic Stress Distribution Surrounding a Running Crack-A Photoelastic Analysis", incl. Disucssion by G. R. Irwin, Proceedings of the Society for Experimental Stress Analysis, Vol. 16. No. 1, 1958, pp. 69-96.

37. Bradley, W. B., and Kobayashi, A. S., "Fracture Dynamics - A Photoelastic Investigation", Journal of Engineering Fracture Mechanics, Vol. 3, No. 3, Oct. 1971, pp. 317-332.

38. Sommer, E., Hodulak, L. and Kordisch, H., "Growth Characteristics of Part-Through Cracks in Thick Walled Plates and Tubes", Journal of Pressure Vessel Technology, Feb. 1977, pp. 106-111.

☆U.S.Government Printing Office: 1979 — 657-002/575